JACS
JOURNAL OF THE AMERICAN CHEMICAL SOCIETY
pubs.acs.org/JACS
Article

Controlling Intramolecular Rotation with Five-Membered Heterocycles Facilitates the Design of Highly Cell-Permeable Xanthene-Based Fluorogenic Probes

Shahi Imam Reja, Yuichiro Hori,* Youhei Takeda, Miyako Nishiura, Masafumi Minoshima, and Kazuya Kikuchi*

Cite This: J. Am. Chem. Soc. 2025, 147, 47997−48012
Read Online

ACCESS | Metrics & More | Article Recommendations | Supporting Information

ABSTRACT: Fluorogenic probes are invaluable tools in biology and medicine, offering high sensitivity and background-free imaging. However, achieving a high signal-to-noise ratio, target specificity, and robust cell permeability in wash-free imaging remains a significant challenge. Here, we report a new class of fluorogenic fluorophores engineered by incorporating five-membered heterocycles such as furan or thiophene at 9-position of the xanthene core. This structural modification enables precise control over intramolecular rotation, which is suppressed in viscous environments or upon interaction with biomolecular targets to allow for fluorescence activation independent of the spirolactone equilibrium characteristic of traditional rhodamine fluorophores. This rotation-based activation strategy was further extended to develop furan- and thiophene-substituted carborhodamine and silicon-rhodamine fluorophores, demonstrating the versatility and modularity of our approach. Using this design, we developed practical fluorogenic probes for self-labeling protein tags, including HaloTag, SNAP-tag, and PYP-tag, achieving high cell permeability and strong fluorescence activation under no-wash live-cell imaging conditions. The HaloTag probe enabled real-time visualization of the endoplasmic reticulum whorl formation in live cells, showcasing its utility in dynamic cellular imaging. To enhance the applicability of our design, we developed BRD4- and EGFR-targeting probes by conjugating our fluorophores with JQ1 and gefitinib/erlotinib inhibitors, utilizing a non-covalent binding strategy. The EGFR-targeting probes exhibited strong fluorescence in cells with high levels of EGFR expression, demonstrating their effectiveness for detecting EGFR overexpression. This work presents a versatile design strategy that leverages the controlled intramolecular rotation of furan/thiophene rings to create innovative OFF/ON fluorogenic probes, offering a robust platform for selective, wash-free live-cell imaging of diverse cellular targets.

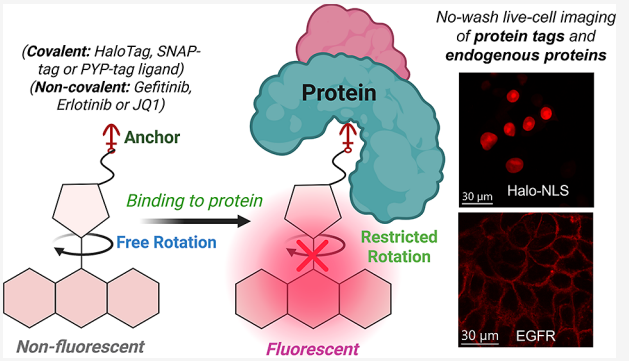

INTRODUCTION

Fluorogenic probes offer straightforward and effective methods for detecting biomolecules in live-cell imaging due to their high sensitivity and ability for background-free imaging.[1−4] A fluorogenic fluorophore coupled with self-labeling protein (SLP) tags, such as HaloTag,[5] SNAP-tag,[6] and PYP-tag,[7] for detection of biomolecules is a useful technology to monitor biomolecules within living cells using fluorescence microscopy.[8,9] In recent years, significant advancements have been achieved in the development of fluorogenic probes,[10−16] which have been successfully utilized across various fields including biosensor development,[17] drug screening,[18] protein function monitoring,[19] and super-resolution imaging.[20] Different design strategies have been employed to create fluorogenic probes, including photoinduced electron transfer (PeT),[21] Förster resonance energy transfer (FRET),[22] intramolecular charge transfer/twisted intramolecular charge transfer (ICT/TICT),[23−25] and intramolecular spirocyclization.[26] Rhodamine dyes have a rich history dating back to their discovery in the 1880s. They have undergone extensive structural modifications over 145 years to attain enhanced photostability, brightness, and fluorogenic responsiveness.[27−36] The most promising fluorogenic probes are developed based on the reversible spirolactone ring-opening and -closing of rhodamine fluorophores,[31−38] taking advantage of their high quantum yield (QY) and photostability. However, at neutral pH, rhodamine-based probes exist in a zwitterionic form in their free state, which limits cell permeability.[39,40]

To achieve high permeability, researchers favor the non-fluorescent hydrophobic spirocyclic state of rhodamine, and

Received: July 24, 2025
Revised: December 7, 2025
Accepted: December 9, 2025
Published: December 16, 2025

https://doi.org/10.1021/jacs.5c12696
J. Am. Chem. Soc. 2025, 147, 47997−48012

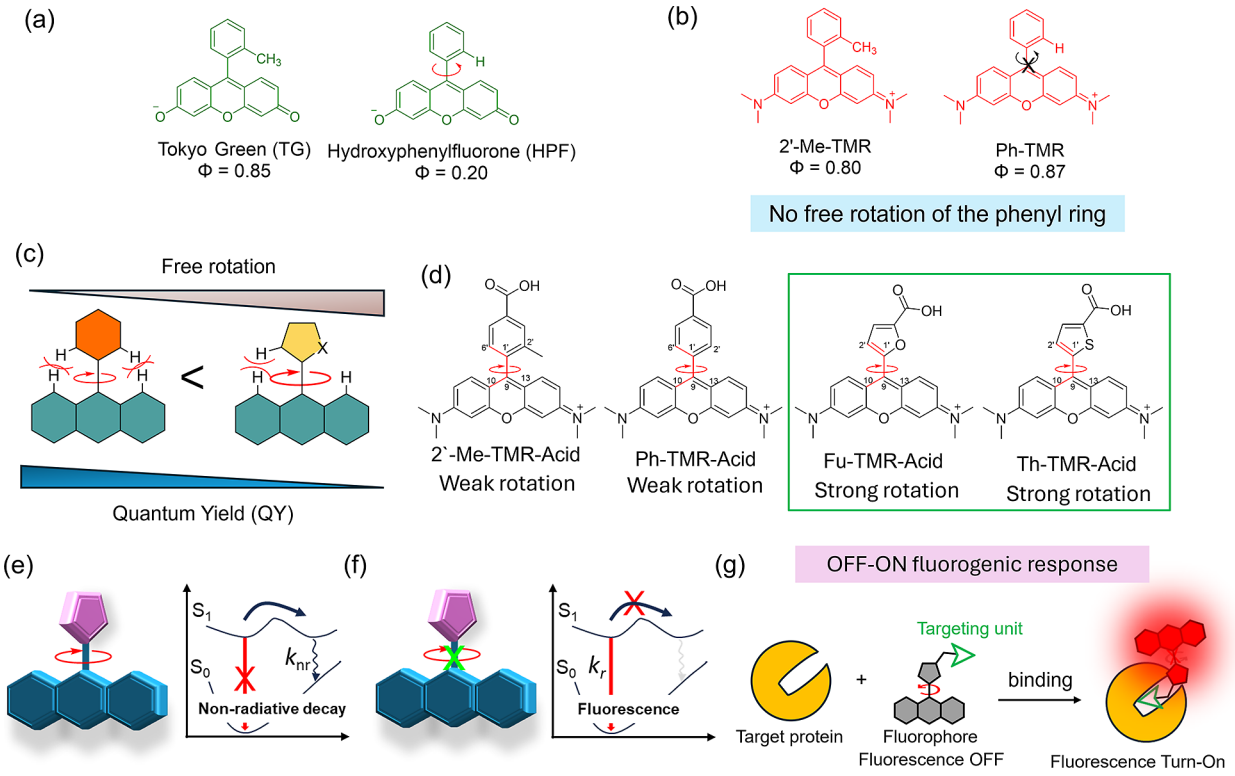

Figure 1. (a) Structures of Tokyo Green and hydroxyphenylfluorone with their QY values measured in 0.1 N NaOH(aq).[50] (b) Structures of 2′-Me-TMR and Ph-TMR with their QY values in ethanol.[51] (c) Schematic representation of the concept: replacing the phenyl ring with a five-membered heterocyclic ring increases rotational freedom. (d) Structures of 2′-Me-TMR-Acid, Ph-TMR-Acid, Fu-TMR-Acid, and Th-TMR-Acid. (e) The OFF−ON fluorophore concept relies on rotational freedom of the ring that facilitates non-radiative pathways. (f) Upon restriction of the ring rotation, the radiative pathway becomes favored, leading to fluorescence activation. (g) Schematic representation of the OFF−ON fluorogenic response through ring rotation restriction that occurs when the fluorophore attached to a protein-targeting unit interacts with the target protein.

numerous valuable cell-permeable rhodamine dyes have been developed to date.[31−36] However, when conjugated to hydrophobic ligands, this state can promote aggregation, leading to cellular toxicity and off-target signals.[41] Moreover, rhodamine fluorophores often emit fluorescence in low-pH environments due to spontaneous ring opening, posing challenges for imaging under acidic conditions.[42,43] To eliminate the pH sensitivity of rhodamine-based fluorophores, a new strategy is needed that does not rely on the fluorogenic response driven by the spirolactone ring-opening and -closing mechanism. The Hanaoka and Urano groups have developed *N*-phenyl rhodamine dyes that do not rely on the traditional spirolactone ring-opening and -closing mechanism for a fluorogenic response.[44] Instead, the fluorescence is quenched due to a twisted intramolecular charge transfer (TICT) state. The TICT state is suppressed when the dye is bound to a protein tag or placed in a highly viscous environment, resulting in enhanced fluorescence emission. This approach also holds promise for the development of pH-insensitive fluorogenic probes. However, these *N*-phenyl rhodamine dye-based probes have sulfonates to avoid nonspecific binding, rendering them impermeable to cellular membranes. Thus, there remains a critical need for a new class of highly cell-permeable, pH-insensitive fluorogenic probes. These probes should be capable of detecting intracellular proteins through covalent and non-covalent interactions to expand their utility in live-cell imaging and protein detection applications.

Here, we present a straightforward and effective strategy for developing a new class of fluorogenic fluorophores by replacing the phenyl ring at the 9-position of the xanthene core with a five-membered heterocycle such as furan or thiophene. This structural modification increases the conformational flexibility of the molecule, facilitating free intramolecular rotation, resulting in a nonfluorescent state. Moreover, fluorescence is strongly activated when this rotation is restricted, either in highly viscous environments or upon binding to biomolecular targets. By precisely controlling the intramolecular rotation of these five-membered heterocycles, we can rationally design fluorogenic probes that respond to a wide range of biological targets. To test the concept, we developed a new class of fluorogenic probes for protein labeling by conjugating these fluorophores with ligands for HaloTag, SNAP-tag, or PYP-tag. These probes exhibited enhanced fluorescence upon binding to protein tags and superior cell permeability that enabled no-wash live-cell imaging for real-time monitoring of protein functions and dynamics. They performed excellently in merged color and long-term imaging. Additionally, the HaloTag-based probe was successfully applied for real-time imaging of endoplasmic reticulum (ER) whorl formation during ER stress,[45] showcasing its utility in dynamic cellular imaging. Furthermore, to explore the use of the fluorophore beyond covalent protein-labeling systems, we developed probes for detecting the overexpression of the epidermal growth factor receptor (EGFR)[46] and bromodomain-containing protein 4 (BRD4),[47] further enhancing the versatility of these newly designed fluorophores. Our results demonstrate that these probes detect EGFR overexpression and BRD4 expression in mammalian cells, offering a promising new strategy for creating

https://doi.org/10.1021/jacs.5c12696
J. Am. Chem. Soc. 2025, 147, 47997−48012

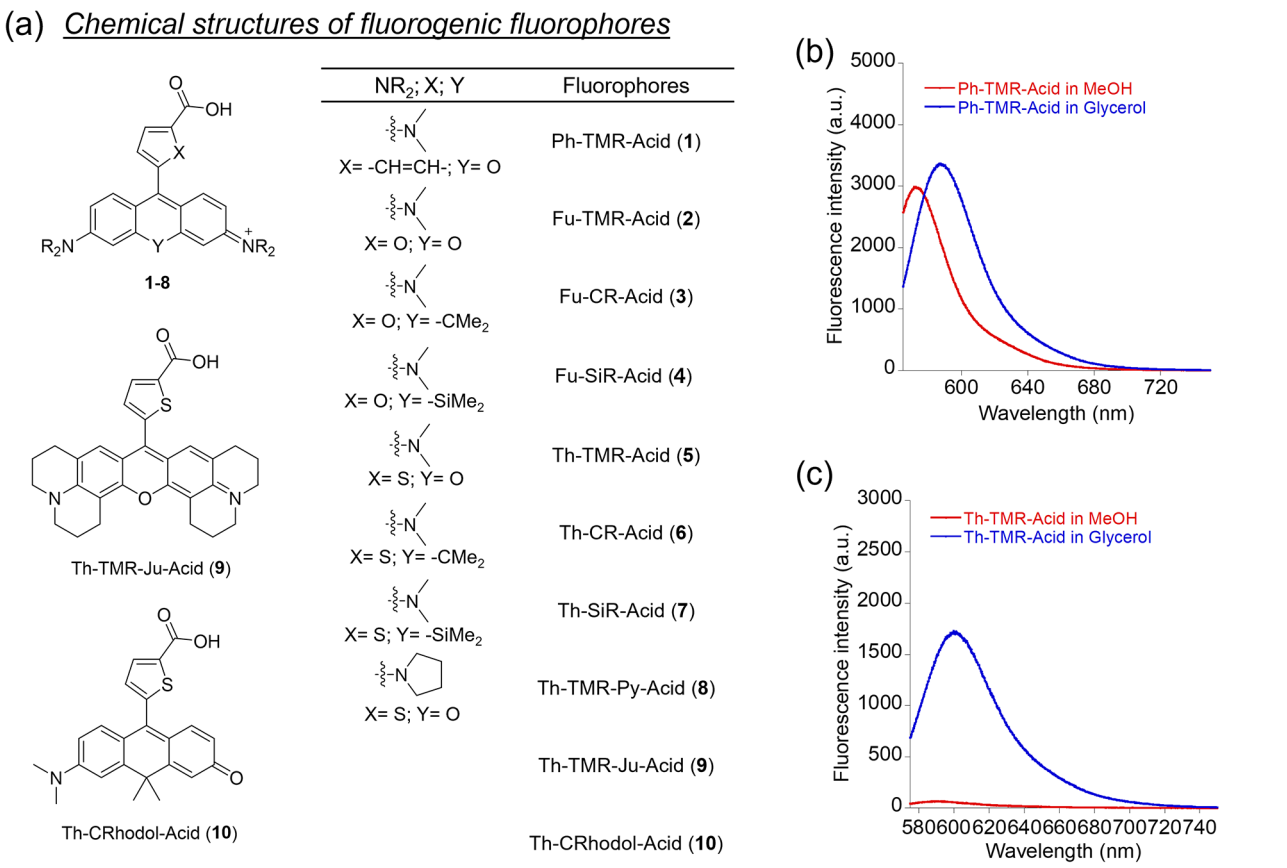

Figure 2. (a) Chemical structures of the fluorophores used in this study. Fluorescence spectra of (b) Ph-TMR-Acid and (c) Th-TMR-Acid (2.5 μM) measured in MeOH (red) and glycerol (blue). Excitation wavelengths: λ_{ex} (Ph-TMR-Acid) = 553 nm; λ_{ex} (Th-TMR-Acid) = 565 nm. All spectra were recorded with 0.25% DMSO as a cosolvent. Temperature: 25 °C.

fluorogenic probes for other intracellular targets. This innovative design is versatile and can be extended to developing a new class of fluorogenic probes or biosensors with enhanced properties.

RESULTS AND DISCUSSION

Rational Design and Photophysical Properties of a Fluorogenic Fluorophore. In 1966, Lindqvist and Lundeen noted that removing the carboxylic acid from fluorescein reduced its QY.[48] Later in 1970, Fink and Wills suggested that this drop in QY was due to energy loss through non-radiative pathways.[49] In 2005, Urano et al. observed a similar effect in Tokyo Green (TG), where removing the 2′-methyl group lowered the QY, likely by permitting rotational motion that dissipated energy nonradiatively (Figure 1a).[50] This led to the belief that the methyl group rigidifies the structure, thus preserving the high fluorescence QY in the fluorophore of the fluorescein analogues. However, in 2021, Arambula et al. demonstrated that rhodamine and rosamine dyes do not follow this trend. They showed that the QY values of the dyes remained unaffected by the same methyl group removal, indicating that rhodamine and rosamine behave differently from fluorescein derivatives (Figure 1b).[51] Based on these findings, we hypothesized that the rhodamine fluorophore with a phenyl ring may not provide adequate rotational freedom at the 9-position of the xanthene core in the excited state due to the involvement of a delocalized electronic state. Hence, we surmised that reducing the steric hindrance at the 9-position, compared to the phenyl ring, could facilitate rotation. This in turn would favor a non-radiative pathway, leading to a significant decrease in fluorescence emission. To investigate the rotational behavior of the phenyl ring at the 9-position of the xanthene core, we first synthesized the phenyl-type fluorophore (Ph-TMR-Acid) and measured the QY in a low-viscosity solvent, MeOH, and a highly viscous solvent, glycerol.[52] The results showed a lower QY value for Ph-TMR-Acid in the less viscous MeOH compared with the highly viscous glycerol (Φ_{MeOH} = 0.33; $\Phi_{Glycerol}$ = 0.66). However, the increase in QY was only 2-fold; thus, we hypothesized that a five-membered ring would introduce a greater angular separation between the xanthene core plane and the five-membered ring, promoting greater rotational freedom. Moreover, removing the interacting hydrogen atom on the phenyl ring of Ph-TMR-Acid by employing a heterocycle was anticipated to further reduce the steric hindrance between the ring and the xanthene core to enhance the conformational flexibility (Figure 1c). Thus, we designed Fu-TMR-Acid and Th-TMR-Acid as fluorogenic fluorophores by substituting the phenyl ring of Ph-TMR-Acid with furan and thiophene rings, respectively (Figure 1d). These specific heterocycles were selected because they have been previously incorporated into nucleobases to develop molecular rotor-based probes, which were later applied in aptamer technology for protein sensing.[53,54]

In low-viscosity environments, Fu-TMR-Acid and Th-TMR-Acid exist in a nonfluorescent state due to non-radiative decay enabled by the free rotation of the furan and thiophene rings (Figure 1e). When this rotation is restricted by increased

https://doi.org/10.1021/jacs.5c12696
J. Am. Chem. Soc. 2025, 147, 47997−48012

viscosity or binding to biomolecules, the non-radiative pathways are suppressed, resulting in strong fluorescence emission (Figure 1f). Therefore, precisely controlling the rotation-dependent fluorescence emission can be leveraged to create fluorogenic probes that remain "OFF" in the unbound state and are switched "ON" upon target binding, enabling the development of an OFF−ON fluorogenic probe for biomolecules (Figure 1g).

To evaluate our fluorogenic design, we first synthesized furan-containing fluorophore Fu-TMR-Acid. Fu-TMR-Acid exhibited a fluorogenic response from MeOH to glycerol, with a noteworthy increase in the QY value in glycerol (Φ_{MeOH} = 0.04; $\Phi_{Glycerol}$ = 0.16) and a 12-fold enhancement in fluorescence intensity. These performances surpass those of the phenyl-type fluorophore Ph-TMR-Acid (Figures 2b, S1, and Table S1). Encouraged by these results, we next synthesized Fu-CR-Acid and Fu-SiR-Acid based on carborhodamine and silicon-rhodamine scaffolds, respectively (Figure 2a). Fu-CR-Acid showed a >17-fold increase in the QY value and a 104-fold enhancement of fluorescence emission in glycerol compared to MeOH, suggesting its potential utility in developing a new class of fluorogenic probes (Figure S1 and Table S1). However, Fu-TMR-Acid and Fu-SiR-Acid showed only 4-fold and 1.3-fold increases in QY from MeOH to glycerol, respectively, indicating a limited fluorogenic response for probe development with these two designs (Figure S1 and Table S1). To improve the fluorogenic response, we selected thiophene as the next five-membered ring for further exploration and synthesized fluorogenic fluorophores, namely, Th-TMR-Acid, Th-CR-Acid, and Th-SiR-Acid. These thiophene-based fluorophores showed 5−25-fold increases in the QY value from MeOH to glycerol (Figures 2c and S1 and Table S1). Moreover, furan/thiophene-based fluorophores exhibited a bathochromic shift in both absorption and emission spectra compared to their phenyl-type analogues due to enhanced coplanarity and extended conjugation with the furan/thiophene ring (Figures S1−S3 and Table S1). To test the generalizability of this fluorophore concept, we synthesized additional TMR-based fluorophores, Th-TMR-Py-Acid and Th-TMR-Ju-Acid, by replacing the dimethylamine moiety of Th-TMR-Acid with pyrrolidine or julolidine, respectively, to suppress the TICT state. Pyrrolidine-based TMR fluorophores are known to exhibit higher QYs than those with dimethylamine.[55] QY measurements of Th-TMR-Py-Acid and Th-TMR-Ju-Acid showed a significant enhancement in glycerol compared to MeOH (Figure S1 and Table S1), indicating that the fluorogenic response is not due to suppression of TICT but rather to restricted rotation of the thiophene ring in a high-viscosity medium. Moreover, we synthesized a rhodol-based fluorophore, Th-CRhodol-Acid, which also showed a weak fluorogenic response from MeOH to glycerol (Figure S4). However, when pH 8 buffer was added to 10% glycerol, the response became more pronounced. Detailed reasoning for this modification is provided in the Supporting Information (Figure S4, Table S1, and SI text page S60). Next, we evaluated the effects of various solvents on the fluorescence behavior of the probes. CR-based fluorophores except for Th-CRhodol-Acid showed a strong fluorescence enhancement in viscous solvents like glycerol, where the high viscosity restricts intramolecular rotations and reduces non-radiative decay, leading to increased fluorescence intensity (Figures S4e and S5). In contrast, TMR-based probes exhibited a moderate fluorescence enhancement in octanol, although it was less pronounced than in glycerol. Intermediate polarity and viscosity of octanol partially restrict the molecular rotation of TMR-based probes and moderately stabilize the excited state. This combination reduces non-radiative decay and influences the fluorescence emission, resulting in increased intensity in octanol with a hypsochromic shift (Figure S5). To assess whether fluorophore aggregation contributed to fluorescence quenching, we measured the fluorescence of the fluorophores in HEPES buffer in the presence of 0.1% SDS as an ionic surfactant. Ph-TMR-Acid displayed an increase in fluorescence intensity, while Fu-TMR-Acid and Th-TMR-Acid showed minimal changes compared with the presence of glycerol (Figures S1 and S3b). These observations suggest that the fluorescence quenching of Fu-TMR-Acid and Th-TMR-Acid is caused by the rotation of the furan/thiophene ring, rather than by aggregation.

To further understand the fluorogenic behavior of the fluorophores, we measured the fluorescence lifetime of all of the fluorophores in MeOH and glycerol (Figure S6). The results revealed that all fluorophores exhibited an increase in fluorescence lifetime from MeOH to glycerol, indicating that the excited state is elongated due to the suppression of non-radiative decay in glycerol (Table S1). To investigate viscosity sensitivity and explore the molecular rotor properties, we calculated both the radiative (k_r) and non-radiative (k_{nr}) pathways for Th-TMR-Acid, as these pathways are crucial for understanding the behavior of molecular rotors.[56] The molecular rotor mainly decays through the k_{nr} pathway, which significantly decreases when rotation is restricted.[57] Upon calculating k_{nr} and k_r, we found a 2.4-fold increase in the radiative (k_r) pathway from MeOH (7×10^7 s^{-1}) to glycerol (1.7×10^8 s^{-1}), while the non-radiative pathway decreased 11.7-fold from MeOH (5.36×10^9 s^{-1}) to glycerol (4.6×10^8 s^{-1}) (Figure S7). The viscosity-insensitive fluorophore Ph-TMR-Acid only showed a 2.7-fold decrease of k_{nr} when moved from MeOH (3.76×10^8 s^{-1}) to glycerol (1.37×10^8 s^{-1}) (Figure S7). This finding indicates that Th-TMR-Acid acts as a fluorescent molecular rotor.

To further investigate the effect of the rotation of the thiophene ring, we performed variable temperature (VT) ^{1}H NMR on Th-TMR-Ju-Acid (Figure S8), which does not exhibit a TICT state (Figure S1 and Table S1). Spectra recorded from 25 °C to −50 °C showed significant downfield shifts in the thiophene ring protons (0.034 ppm in H_a and 0.011 ppm in H_b), while the xanthene core proton remained nearly unchanged (0.002 ppm in H_c). These downfield shifts suggest that rapid rotation of the thiophene ring reduces the level of conjugation with the xanthene core at higher temperatures. At lower temperatures, the thiophene ring rotation becomes restricted and adopts a more coplanar conformation, enhancing conjugation with the xanthene core. This increased conjugation alters the electron density in the thiophene ring, resulting in reduced shielding of the thiophene protons, which in turn leads to the observed downfield shifts due to deshielding effects (see the supplementary text above Figure S8).

Furthermore, we explored the reactivity of the newly designed fluorophores with reduced glutathione (GSH), as the 9-position of the xanthene core is known to be vulnerable to GSH nucleophilicity.[58] Th-TMR-Acid and its structural derivatives showed no reactivity toward GSH (20 mM) (Figure S9). By contrast, Fu-CR-Acid, Fu-SiR-Acid, Th-CR-Acid, and Th-SiR-Acid exhibited reactivity with GSH. Among

https://doi.org/10.1021/jacs.5c12696
J. Am. Chem. Soc. 2025, 147, 47997−48012

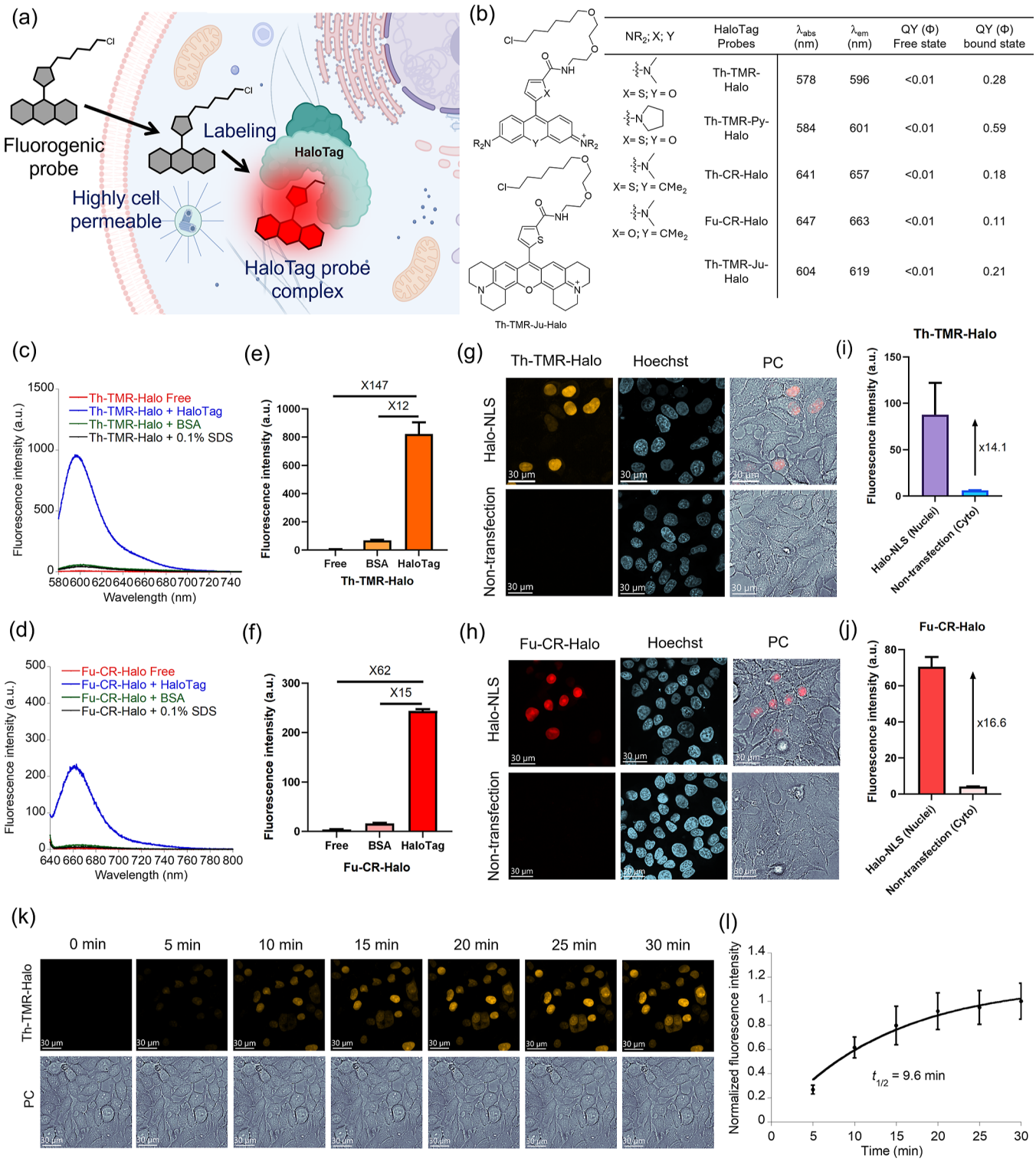

NR_2; X; Y	HaloTag Probes	λ_{abs} (nm)	λ_{em} (nm)	QY (Φ) Free state	QY (Φ) bound state
X= S; Y = O	Th-TMR-Halo	578	596	<0.01	0.28
X= S; Y = O	Th-TMR-Py-Halo	584	601	<0.01	0.59
X= S; Y = CMe_2	Th-CR-Halo	641	657	<0.01	0.18
X= O; Y = CMe_2	Fu-CR-Halo	647	663	<0.01	0.11
	Th-TMR-Ju-Halo	604	619	<0.01	0.21

Figure 3. (a) Schematic representation of the intracellular fluorogenic response of the HaloTag probe. (b) Structures of HaloTag probes with their quantum yield (QY) values in the free and bound states, along with absorption (λ_{abs}) and emission (λ_{em}) maximum wavelengths in the bound state. (c, d) Emission spectra of Th-TMR-Halo and Fu-CR-Halo (2.5 μM) in the absence (red) or presence of HaloTag (5 μM) (blue) or 0.1% SDS (black) or BSA (20 μM) (green) in 20 mM HEPES buffer, 150 mM NaCl, pH 7.4; λ_{ex} (Th-TMR-Halo) = 570 nm; λ_{ex} (Fu-CR-Halo) = 635 nm. (e, f) Fluorescence intensity of (e) Th-TMR-Halo and (f) Fu-CR-Halo with the free state and in the presence of BSA and HaloTag. (g, h) Live-cell confocal fluorescence images of MCF7 cells expressing the Halo-NLS gene or non-transfected cells with 500 nM (g) Th-TMR-Halo and (h) Fu-CR-Halo, costained with 1.0 μg/mL Hoechst. (i, j) The intensity analysis of (i) Th-TMR-Halo and (j) Fu-CR-Halo in the Halo-NLS-expressing (nuclei) and non-transfected cells (cytosol). For Th-TMR-Halo: $N_{(Nuclei)}$ = 13 cells; $N_{(Cyto)}$ = 11 cells. For Fu-CR-Halo: $N_{(Nuclei)}$ = 12 cells; $N_{(Cyto)}$ = 10 cells (λ_{ex} = 405/561/638 nm, λ_{em} = 435−455 nm for Hoechst; 580−610 nm for Th-TMR-Halo; 671−745 nm for Fu-CR-Halo). (k) Time-lapse images of Th-TMR-Halo (500 nM) in MCF7 cells expressing the Halo-NLS gene (λ_{ex} = 561 nm, λ_{em} = 580−610 nm). 0 min indicates before the addition of Th-TMR-Halo. (l) Normalized fluorescence intensity of Th-TMR-Halo at each time point. The error bar denotes mean ± SD; N = 10 cells at each time point. PC: phase contrast.

https://doi.org/10.1021/jacs.5c12696
J. Am. Chem. Soc. 2025, 147, 47997−48012

these fluorophores, Fu-SiR-Acid and Th-CR-Acid were relatively more stable than others under reducing conditions (Figure S9). After assessing the QY in glycerol and GSH sensitivity, we identified five fluorophores (Th-TMR-Acid, Th-TMR-Py-Acid, Th-TMR-Ju-Acid, Th-CR-Acid, and Fu-CR-Acid) as optimal candidates for probe development and further investigations (Figures 2 and S9 and Table S1). Next, we evaluated the viscosity sensitivity of the fluorophores over a range of viscosities from 17 cP to 560 cP using the Förster–Hoffmann equation ($\log I = x \log \eta + C$),[59,60] where I represents the fluorescence intensity, x denotes the viscosity sensitivity, η indicates the solvent viscosity, and C is a constant (Figure S10). All five fluorophores displayed strong linear relationships between the solvent viscosity and fluorescence intensity. The slope of the linear region was $x = 0.55$ ($R^2 = 0.99$) for Th-TMR-Acid, 0.49 ($R^2 = 0.99$) for Th-TMR-Py-Acid, 0.45 ($R^2 = 0.99$) for Th-TMR-Ju-Acid, 0.51 ($R^2 = 0.97$) for Th-CR-Acid, and 0.55 ($R^2 = 0.98$) for Fu-CR-Acid. These values are comparable to those for BODIPY-based fluorescent molecular rotors,[61] making them suitable candidates for probe development. In contrast, Ph-TMR-Acid, with $x = 0.03$ ($R^2 = 0.57$), showed insensitivity to the viscosity of the solvent.

Development of Fluorogenic Probes for HaloTag. To validate the concept and practical utility of our fluorogenic fluorophores, we designed probes by attaching them to ligands for self-labeling protein tags such as HaloTag, SNAP-tag, and PYP-tag. We first developed HaloTag-based probes for the initial evaluation of the fluorogenic response and cell permeability. HaloTag probes are initially nonfluorescent due to free rotation of the furan/thiophene ring, but binding to HaloTag restricts this rotation, enhancing fluorescence intensity (Figure 3a). After conjugating HaloTag ligands to fluorophores, we created Th-TMR-Halo, Th-TMR-Py-Halo, Th-TMR-Ju-Halo, Fu-CR-Halo, and Th-CR-Halo, covering red to far-red emission (Figure 3b). As expected, all of the HaloTag probes demonstrated a pronounced fluorogenic response in the presence of recombinant HaloTag, showing fluorescence signal enhancements of up to 147-, 149-, 144-, 62-, and 54-fold for Th-TMR-Halo, Th-TMR-Py-Halo, Th-TMR-Ju-Halo, Fu-CR-Halo, and Th-CR-Halo, respectively (Figures 3c–f, S11, and S12). Moreover, all of the HaloTag probes exhibited a greater than 11-fold enhancement in QY upon binding to the HaloTag (Figure 3b). We also tested off-target binding by exposing HaloTag probes to bovine serum albumin (BSA) (20 μM). Except for Th-TMR-Ju-Halo, only a minimal fluorescence increase was observed, indicating low off-target binding (Figures 3c–f, S11, and S12). In addition, we observed negligible fluorescence enhancement in the presence of other proteins, indicating that HaloTag probes exhibited high target selectivity (Figure S13). The labeling specificity was further confirmed in cell lysates, which demonstrated scarce off-target binding to other cellular proteins (Figure S14). Fluorescence measurements in the presence of 0.1% sodium dodecyl sulfate (SDS) showed no significant enhancement, indicating that probe quenching was not due to aggregation and confirming high selectivity for target proteins (Figures 3c–f, S11, and S12). The labeling reactions for HaloTag were confirmed by SDS–polyacrylamide gel electrophoresis (PAGE) analysis (Figure S15). Moreover, the fluorescence spectra of HaloTag-labeled Th-TMR-Halo were recorded under denaturing conditions upon the addition of a 1% SDS solution, resulting in a 14-fold decrease in fluorescence intensity (Figure S16). This confirms the probe's sensitivity to the intact protein tag. Moreover, we tested our HaloTag probes (Th-TMR-Halo, Th-TMR-Py-Halo, Th-CR-Halo, and Fu-CR-Halo) for pH sensitivity. The free probes did not exhibit pH sensitivity, nor did the probes labeled with HaloTag across the pH range of 5–8, indicating their applicability in a broad pH range (Figure S17). Next, we measured the second-order rate constants (k_2) of Th-TMR-Halo, Th-TMR-Py-Halo, Th-TMR-Ju-Halo, Th-CR-Halo, and Fu-CR-Halo for binding to HaloTag. The results showed k_2 values ranging from 5.6×10^3 to 2.8×10^4 M^{-1} s^{-1} of HaloTag probes, which are all sufficiently fast and suitable for practical applications (Figure S18).

To evaluate HaloTag probes for intracellular labeling, we applied Th-TMR-Halo, Th-TMR-Py-Halo, Th-TMR-Ju-Halo, Fu-CR-Halo, and Th-CR-Halo to no-wash live-cell imaging of MCF7 cells transiently expressing a HaloTag called HA-Halo-NLS[62] in the cell nuclei. Using a no-wash imaging protocol with confocal fluorescence microscopy, we observed bright fluorescence signals from the nuclei of cells expressing HA-Halo-NLS, while non-transfected cells or those not expressing the HaloTag showed negligible fluorescence (Figures 3g,h and S19). Upon calculating the nucleus-to-cytosol ratio, we found that Th-TMR-Halo, Th-TMR-Py-Halo, Th-TMR-Ju-Halo, Fu-CR-Halo, and Th-CR-Halo demonstrated 14.1-, 8.3-, 3.5-, 16.6-, and 6.6-fold increases in fluorescence intensity in the nuclei of cells transiently expressing the HaloTag compared to the cytosol of non-transfected cells (Figures 3i,j and S19). Among the five HaloTag probes, Th-TMR-Halo and Fu-CR-Halo showed the strongest fluorogenic responses in live cells. Time-lapse imaging detected significant fluorescence within 10 min of incubation with 500 nM HaloTag probes, indicating rapid cell permeability and efficient intracellular labeling ($t_{1/2}$ in the cell (Th-TMR-Halo) = 9.6 min) (Figures 3k,l and S20). Furthermore, HaloTag probes were capable of providing sufficient signal intensity below 200 nM in live-cell no-wash imaging (Figures S21–S23). We also tested Th-TMR-Halo at 5 and 10 nM, where it still produced a detectable signal (Figure S24), demonstrating its sensitivity at low concentrations. Moreover, Th-TMR-Halo and Fu-CR-Halo showed fluorescence signals from nuclei after labeling at higher concentrations (5 μM, 10 μM, and 20 μM) without washing, confirming their target specificities (Figure S25). Extended imaging with Fu-CR-Halo using a wash protocol showed a bright signal persisted over 6 h, demonstrating its suitability for long-term protein tracking in live cells (Figure S26). Comparison of the fluorogenic response of Th-TMR-Halo with that of TMR-Halo, a commercially available HaloTag probe, revealed that Th-TMR-Halo was 7.8-fold brighter than TMR-Halo at the same concentration (Figure S27). This enhanced fluorescence intensity of Th-TMR-Halo is likely due to its greater cell permeability. TMR-Halo exists in a zwitterionic form at neutral pH, which reduces its cell permeability. Moreover, to evaluate the ability of the probes to detect HaloTag in different organelles, we expressed HaloTag in various locations, including the ER (Halo-Sec61β[63]), mitochondria (COX8-Halo-mCherry[64]), and cytoplasm (MBP-Halo-mCherry[64]). Th-TMR-Halo, Th-TMR-Py-Halo, Fu-CR-Halo, and Th-CR-Halo were used to detect HaloTag in the ER (Figure S28a). Th-CR-Halo and Fu-CR-Halo were used to detect HaloTag in the mitochondria (Figure S28b,c), while MBP-Halo-mCherry was used for cytoplasmic detection (Figure S28d). In the mitochondria and cytoplasm, HaloTags were coexpressed with mCherry to show perfect

https://doi.org/10.1021/jacs.5c12696
J. Am. Chem. Soc. 2025, 147, 47997–48012

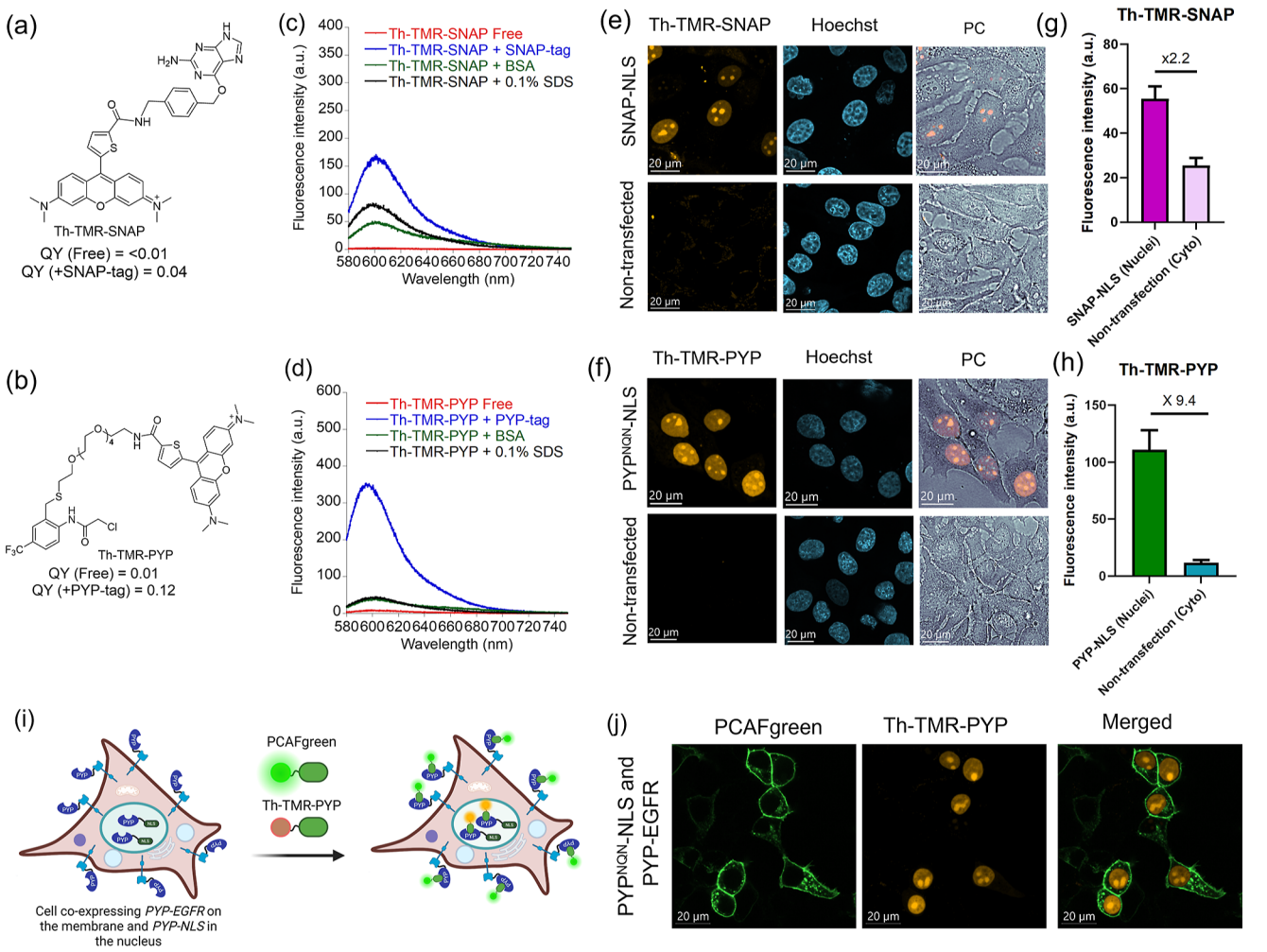

Figure 4. Structures of (a) the SNAP-tag and (b) the PYP-tag probes. Emission spectra of (c) Th-TMR-SNAP (2.5 μM) and (d) Th-TMR-PYP (2.5 μM) in the absence (red) and presence of SNAP-tag/PYP-tag (5 μM) (blue), 0.1% SDS (black), or BSA (20 μM) (green) in 20 mM HEPES buffer, 150 mM NaCl, pH 7.4; λ_{ex} = 570 nm. (e, f) Live-cell confocal fluorescence images of MCF7 cells expressing the (e) SNAP-NLS gene or non-transfected cells with 1.0 μM Th-TMR-SNAP and (f) PYP^{NQN}-NLS or non-transfected cells with 1.0 μM Th-TMR-PYP, preincubated with 1.0 μM MitoTracker Deep Red for 10 min, and costained with 1.0 μg/mL Hoechst. (g) The intensity analysis of Th-TMR-SNAP in the SNAP-NLS-expressing (nuclei) and non-transfected (cytosol) cells: $N_{(Nuclei)}$ = 10 cells; $N_{(Cyto)}$ = 10 cells. (h) The intensity analysis of Th-TMR-PYP in the PYP^{NQN}-NLS-expressing (nuclei) and non-transfected (cytosol) cells: $N_{(Nuclei)}$ = 9 cells; $N_{(Cyto)}$ = 9 cells. For (e, f) λ_{ex} = 405/561 nm, λ_{em} = 435–455 nm for Hoechst; 580–610 nm for Th-TMR-SNAP and Th-TMR-PYP. (i) Schematic representation of merged color imaging of PYP probes on the cell surface (PYP^{wt}-EGFR) and inside the cell (PYP^{NQN}-NLS) using PCAFgreen and Th-TMR-PYP. (j) Live-cell dual-color imaging of HEK293T cells expressing the PYP^{wt}-EGFR and PYP^{NQN}-NLS genes using PCAFgreen (1.0 μM) and Th-TMR-PYP (1.0 μM), preincubated with 1.0 μM MitoTracker Deep Red for 10 min. PC: phase contrast.

colocalization with labeling by the HaloTag probes. The imaging data demonstrate the utility of the probes for the no-wash imaging of intracellular HaloTag in different cell compartments.

Fluorogenic Probes for SNAP-Tag and PYP-Tag. Following the successful fluorogenic response of the HaloTag-based probes, we synthesized fluorogenic probes for other self-labeling protein tags, such as SNAP-tag and PYP-tag by conjugating Th-TMR-Acid with their ligands, creating Th-TMR-SNAP and Th-TMR-PYP, respectively (Figure 4a,b). Both probes exhibited fluorogenic responses and a >4-fold increase in QY in the presence of their respective protein tags (Φ_{Free} = < 0.01; Φ_{bound} = 0.04 for Th-TMR-SNAP; Φ_{Free} = 0.01; Φ_{bound} = 0.12 for Th-TMR-PYP) (Figures 4a–d and S29 and Table S3). The labeling of the tags with the probes was confirmed by SDS–PAGE analysis (Figure S30). To expand structural diversity, we also developed Th-TMR-Py-SNAP and Th-CR-SNAP probes, both of which exhibited fluorogenic responses upon binding to the SNAP-tag (Figure S31 and Table S3). However, all SNAP-tag probes showed nonspecific fluorescence enhancement in the presence of BSA (20 μM) (Figures 4c and S31).

Additionally, increased fluorescence emission in the presence of 0.1% SDS suggests the possible aggregation of free probes in HEPES buffer (Figures 4c and S31). On the other hand, Th-TMR-PYP did not exhibit significant non-specific binding to BSA or an increase in fluorescence in the presence of 0.1% SDS (Figures 4d and S29). We next evaluated the SNAP-tag and PYP-tag probes under no-wash live-cell imaging conditions. MCF7 cells transiently expressed SNAP-NLS or PYP^{NQN}-NLS in nuclei. Upon incubation with Th-TMR-SNAP or Th-TMR-PYP, we can detect the fluorescence signal from the nuclei along with a nonspecific signal due to mislocalization of probes into mitochondria

https://doi.org/10.1021/jacs.5c12696
J. Am. Chem. Soc. 2025, 147, 47997–48012

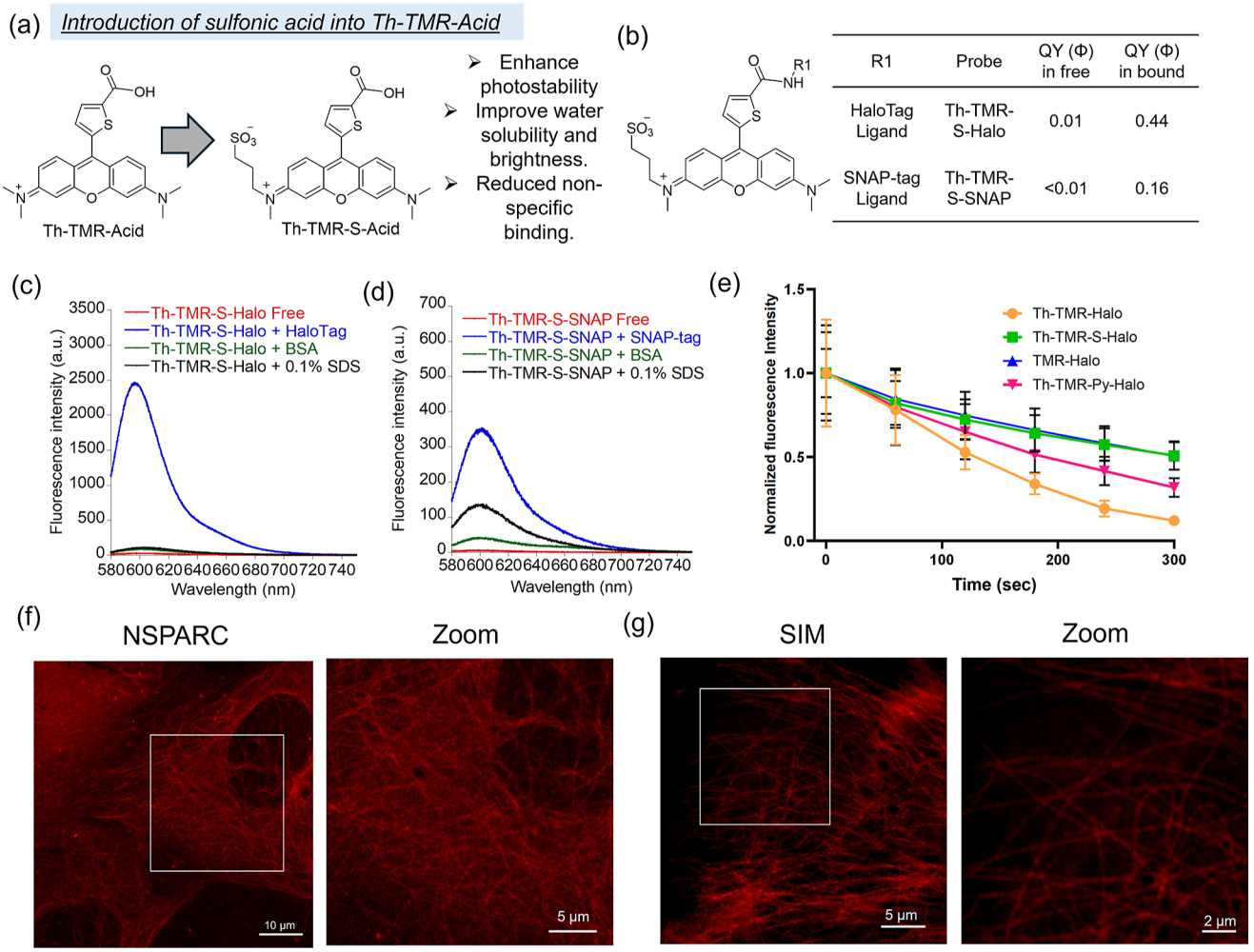

Figure 5. (a) Structures of Th-TMR-Acid and its derivative Th-TMR-S-Acid where a sulfonic acid group is introduced for improved photostability, water solubility, and brightness. (b) Chemical structures of Th-TMR-S-Halo and Th-TMR-S-SNAP with their QY values in the free and bound states. Emission spectra of (c) Th-TMR-S-Halo and (d) Th-TMR-S-SNAP (2.5 μM) in the absence (red) and presence of HaloTag/SNAP-tag (5 μM) (blue), 0.1% SDS (black), or BSA (20 μM) (green) in 20 mM HEPES buffer, 150 mM NaCl, pH 7.4; λ_{ex} (Th-TMR-S-Halo and Th-TMR-S-SNAP) = 570 nm. (e) Normalized fluorescence intensity of each probe for each time point. Continuous yellow laser (4.7 mW) irradiation for 60 s was given for each time point. The error bar represents mean ± SD (N = 12 cells for Th-TMR-Halo, TMR-Halo, and Th-TMR-S-Halo; N = 15 cells for Th-TMR-Py-Halo). (f) No-wash super-resolution NSPARC image of live U2OS cells expressing the tubulin-Halo gene with 500 nM Th-TMR-S-Halo. λ_{ex} = 561 nm; λ_{em} = 570−616 nm. Scale bar: 10 and 5 μm (zoom). (g) No-wash super-resolution N-SIM image of fixed COS7 cells expressing the tubulin-Halo gene with 10 nM Th-TMR-S-Halo. λ_{ex} = 561 nm; λ_{em} = 620 nm. Scale bar: 5 and 2 μm (zoom).

(Figure S32). However, costaining with MitoTracker dyes (MitoTracker Deep Red, hereafter MTDR)[65] significantly improved the signal-to-noise ratio of these probes for the no-wash imaging protocol (Figure 4e,f). While Th-TMR-SNAP exhibited only a 2.2-fold enhancement of the nucleus-to-cytosol ratio (Figure 4g), Th-TMR-PYP showed a 9.4-fold enhancement (Figure 4h). We also found markedly reduced mitochondrial accumulation of the SNAP-tag probe Th-TMR-SNAP upon preincubation with carbonyl cyanide-*p*-trifluoromethoxyphenylhydrazone (FCCP), a nonfluorescent ionophore that transports proton to disrupts ATP synthesis in mitochondria (Figure S33).[66] Th-TMR-PYP labeled only the intracellular inner membrane protein (Lyn_{11}-PYP^{wt}) but not the extracellular surface protein (PYP^{wt}-EGFR). This indicates its high cell permeability and selectivity for intracellular proteins (Figure S34), which is similar to the probes we previously developed.[67] Such localization selectivity enables multicolor imaging using distinct fluorophores with different emission spectra that allows simultaneous visualization of multiple targets or structures.[68] Thus, we performed dual-color imaging of PYP-tag probes in HEK293T cells cotransfected with the PYP^{wt}-EGFR and PYP^{NQN}-NLS genes (Figure 4i). Upon labeling with a cell-impermeable probe PCAFgreen[66] and a cell-permeable probe Th-TMR-PYP, PCAFgreen specifically labeled PYP^{wt}-EGFR on the cell surface, whereas Th-TMR-PYP selectively labeled the intracellular protein in the nucleus (Figure 4j).

Evolution of Highly Photostable and Improved Fluorogenic Probes for HaloTag and SNAP-Tag. The photostability of Th-TMR-Halo, Th-TMR-Py-Halo, and TMR-Halo was evaluated by live-cell imaging under continuous laser irradiation in MCF7 cells expressing Halo-NLS (Figure S35). The data showed that both Th-TMR-Halo and Th-TMR-Py-Halo exhibited poorer photostability compared to TMR-Halo, indicating a need for further improvement (Figure S35). Previous studies have shown that introduction of sulfonic acid groups can enhance the photostability of fluorophores.[69] In addition, a recently reported cell-permeable probe conjugated

https://doi.org/10.1021/jacs.5c12696
J. Am. Chem. Soc. 2025, 147, 47997−48012

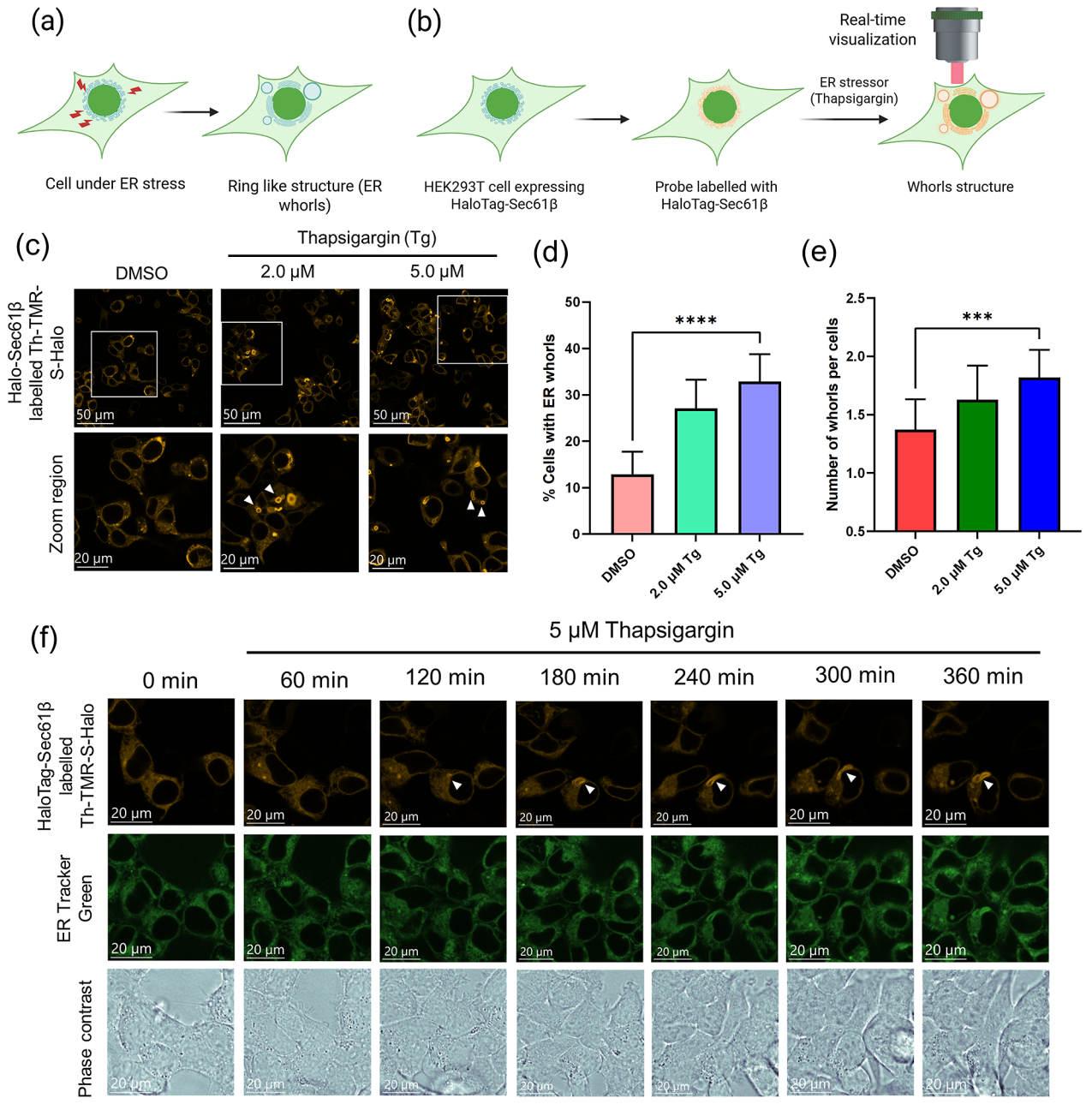

Figure 6. (a) Schematic illustration of ER whorl formation in response to ER stress. (b) Diagram showing HEK293T cells expressing Halo-Sec61β, labeled with a HaloTag probe and treated with thapsigargin (Tg) to visualize ER whorls in live cells. (c) Live-cell imaging of ER whorls in HEK293T cells expressing Halo-Sec61β labeled with 500 nM Th-TMR-S-Halo after treated with DMSO, 2.0 μM Tg, or 5.0 μM Tg for 6 h. Zoomed-in regions highlight ER whorls (indicated by white arrows). Cells were incubated with Th-TMR-S-Halo for 60 min and washed with HBSS buffer before treatment. (d) Quantification of the percentage of cells exhibiting ER whorls across treatment groups (DMSO, 2.0 μM Tg, and 5.0 μM Tg). (e) Number of ER whorls per ER whorl-positive cell. Error bars represent standard deviation (SD) from three independent experiments. Statistical significance: ****$p < 0.0001$, ***$p < 0.001$. (f) Time-lapse live-cell imaging of Halo-Sec61β labeled with Th-TMR-S-Halo (yellow) in the presence of 5.0 μM Tg and 1.0 μM ER-Tracker Green (green). Time 0 min indicates the point just before Tg addition (λ_{ex} = 488/561 nm, λ_{em} = 517−541 nm for ER Tracker Green and 580−610 nm for Th-TMR-S-Halo).

with sulfonic acid demonstrated improved water solubility.[70] Based on these findings, we hypothesized that applying a similar strategy could improve the photostability of Th-TMR-Halo and reduce the nonspecific binding observed with our SNAP-tag probe. Thus, considering the above advantages, we synthesized a sulfonic-acid-linked Th-TMR-Acid fluorophore, designated as Th-TMR-S-Acid, to enhance both photostability and water solubility (Figure 5a). The fluorophore demonstrated a high molar absorption coefficient due to high solubility and showed a similar fluorogenic response from MeOH to glycerol (Φ_{MeOH} = 0.02; $\Phi_{Glycerol}$ = 0.31) and viscosity sensitivity x = 0.45 (R^2 = 0.99) (Figure S36 and Table S1). Th-TMR-S-Acid exhibited a 2-fold increase in brightness in glycerol compared with Th-TMR-Acid, indicating its suitability for probe development (Table S1). Thus, we conjugated Th-TMR-S-Acid with HaloTag and SNAP-tag ligands and created Th-TMR-S-Halo and Th-TMR-S-SNAP, respectively. Th-TMR-S-Halo performed exceptionally well,

https://doi.org/10.1021/jacs.5c12696
J. Am. Chem. Soc. 2025, 147, 47997−48012

displaying a fluorogenic response superior to that of Th-TMR-Halo in the presence of HaloTag (Φ_{Free} = 0.01; Φ_{bound} = 0.44) (Figures 5b,c, S37, and S38 and Table S2). Moreover, Th-TMR-S-SNAP exhibited reduced nonspecific binding to BSA and improved fluorogenic response in the presence of the SNAP-tag protein (Φ_{Free} = < 0.01; Φ_{bound} = 0.16) (Figures 5b,d and S39 and Table S3). Although all the SNAP-tag probes functioned as fluorogenic probes, further modifications or the second-generation SNAP-tag protein or ligand (SNAP-tag2)[71] could enhance the performance.

To assess the cell permeability of the sulfonic acid-conjugated probes, we transiently expressed HaloTag (Halo-NLS) or SNAP-tag (SNAP-NLS) in MCF7 cells and incubated the cells with Th-TMR-S-Halo or Th-TMR-S-SNAP for 1.5 h. Following cell washing in HBSS buffer, the cell lysates were analyzed by SDS−PAGE, revealing fluorescence signals for both probes (Figure S40). These results confirmed that the probes are membrane-permeable and effectively label intracellular proteins. Moreover, the cytotoxicity assay indicated that the introduction of a sulfonic acid group into the probe does not cause any detectable toxicity to the cells (Figure S41). Time-lapse imaging of Th-TMR-S-Halo in cells expressing HaloTag inside the cell nuclei revealed a slower labeling reaction ($t_{1/2incell(Th\text{-}TMR\text{-}S\text{-}Halo)}$ = 39 min) (Figure S42), approximately four times slower than Th-TMR-Halo, likely due to the reduced cellular permeability of the sulfonated probe. However, Th-TMR-S-Halo exhibited a 16.2-fold increase in the fluorescence intensity with transiently expressed HaloTag within the nuclei compared to the cytosol of non-transfected cells, outperforming Th-TMR-Halo (Figure S43). Moreover, Th-TMR-S-Halo successfully visualized the cytoskeleton in U2OS cells expressing tubulin-Halo (TUBB5-Halo),[72] showing strong colocalization with the commercial tubulin probe SiR-Tubulin (Figure S44). Finally, we evaluated the photostability of Th-TMR-S-Halo to see if introduction of the sulfonic acid group significantly improved the photostability of Th-TMR-Halo. The photostability of Th-TMR-S-Halo was better than that of Th-TMR-Halo and comparable to that of TMR-Halo, suggesting its potential suitability for super-resolution imaging (Figures 5e and S35).[73,74] Using U2OS or COS7 cells expressing tubulin-Halo, we performed no-wash super-resolution imaging using a confocal microscope with a super-resolution detector (NSPARC)[75] for live cells and Super-Resolution Structured Illumination Microscopy (SIM)[76] for fixed cells. Th-TMR-S-Halo clearly visualized the tubulin network in both live and fixed cells under no-wash conditions, revealing the cytoskeletal structures with high spatial resolution (Figures 5f,g and S45).

To evaluate Th-TMR-S-SNAP for live-cell imaging, we expressed SNAP-tag in the nuclei of MCF7 cells and incubated with the probe for 60 min. Under no-wash conditions, a clear nuclear signal was observed, along with mild nonspecific membrane staining (Figure S46). Although Th-TMR-S-SNAP successfully labeled intracellular SNAP-tag, its signal was weaker than Th-TMR-SNAP, likely due to reduced cell permeability. We next applied Th-TMR-S-SNAP to imaging cell-surface SNAP-tag proteins using the no-wash protocol. HEK293T cells transiently expressing the SNAP-tagged β2 adrenergic receptor (SNAP-tag-ADRβ2) were incubated with Th-TMR-S-SNAP. Confocal fluorescence imaging was successfully performed without removing the excess unreacted probe, enabling clear visualization of the cell surface with the SNAP-tagged protein-expressing cells, while non-transfected cells showed a negligible fluorescence signal (Figure S47). Moreover, dual-color imaging was performed by using the HaloTag and SNAP-tag probes. A SiR-SNAP−Th-TMR-S-Halo pair or a Th-TMR-S-SNAP−Fu-CR-Halo pair was used against cells expressing HaloTag and SNAP-tag in different cellular compartments with a no-wash imaging protocol. Under these conditions, we successfully obtained merged color images using the two probes with distinct emission spectra, demonstrating that the newly developed probes are promising candidates for the simultaneous detection of multiple targets without crosstalk (Figure S48).

Real-Time Imaging of ER Whorl Formation during ER Stress. After developing protein-labeling probes, we used the HaloTag probe and developed Th-TMR-S-Halo to study dynamic ER whorl formation under stress. ER is a crucial organelle responsible for protein synthesis, folding, and quality control, playing a vital role in maintaining cellular homeostasis.[77−79] ER whorls are large, ring-like structures that are formed under ER stress (Figure 6a). They can be visualized by labeling ectopically expressed Sec61β, a key component of the Sec61 translocon complex.[80] To enable real-time monitoring of ER whorl formation, we applied the Th-TMR-S-Halo probe. We chose HEK293T cells, as they have been shown to form ER whorls when exposed to stressors like thapsigargin (Tg).[81] To visualize the localization of HaloTag within the ER, we transiently expressed Halo-Sec61β in HEK293T cells and labeled the cells with Th-TMR-S-Halo (Figure 6b). Cells were then treated with 0, 2, or 5 μM Tg and incubated for 6 h. Live-cell confocal microscopy revealed prominent ER whorl formation, consistent with the previous studies[81] (Figure 6c). In the DMSO control group, 12.9 ± 4.9% of cells exhibited ER whorls, whereas treatment with 2 and 5 μM Tg resulted in whorl formation in 27.1 ± 6.2% and 32.9 ± 5.9% of cells, respectively (Figure 6d). Some ER whorl structures were observed in DMSO-treated control cells, likely due to transient transfection-induced stress.

We further calculated the number of whorls per whorl-positive cell, which indicated that the addition of Tg significantly increased the number of whorls per cell (Figure 6e). To further investigate this phenomenon, we performed long-term live-cell imaging over 6 h following the addition of 5.0 μM Tg to monitor the dynamics of ER whorl formation. The time-lapse images visualized the dynamic formation of ER whorls, demonstrating a clear benefit of our probe for monitoring protein dynamics (Figure 6f). While the commercially available ER-Tracker Green can also detect the ER whorls, it is less feasible for monitoring dynamic events (Figure 6f). Furthermore, we were also successful in imaging the ER whorls without washing using Th-TMR-S-Halo, visualizing the formation of ring-like whorls (Figure S49). Thus, this newly developed probe enables real-time visualization of the ER whorl formation, offering practical insights into this dynamic process.

Expanding the Applications of Fluorogenic Fluorophores Using Non-covalent Binding. Following the successful application of our fluorogenic fluorophores with self-labeling protein tags, we sought to apply them to non-covalent protein detection under no-wash conditions. Existing SiR- or TMR-based fluorophores struggle to detect EGFR when linked to ligands like erlotinib.[70] Developing fluorogenic probes for non-covalent detection would expand their use in imaging intracellular targets. To demonstrate this, we targeted two proteins: intracellular BRD4 and membrane-bound EGFR

https://doi.org/10.1021/jacs.5c12696
J. Am. Chem. Soc. 2025, 147, 47997−48012

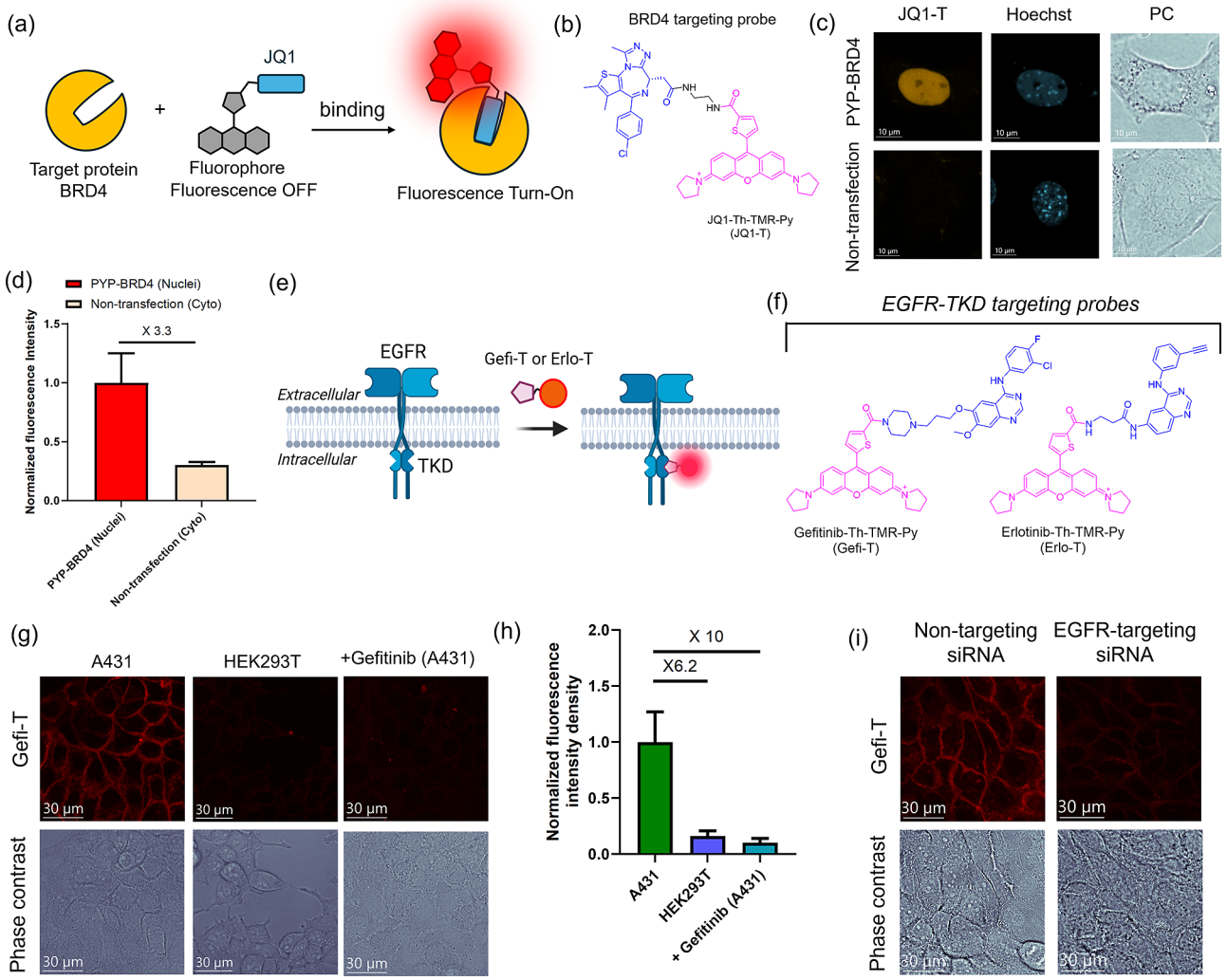

Figure 7. (a) Schematic representation of the OFF−ON-based fluorogenic strategy for detection of bromodomain-containing protein 4 (BRD4). (b) Structure of the BRD4 targeting probe JQ1-Th-TMR-Py (JQ1-T). (c) Live-cell confocal fluorescence images of PYP-BRD4-expressing or non-expressing NIH3T3 cells with 500 nM JQ1-Th-TMR-Py, preincubated with 2.0 μM MitoTracker Deep Red for 10 min, costained with 1.0 μg/mL Hoechst (λ_{ex} = 405/561 nm and λ_{em} = 435−455 nm for Hoechst, 580−610 nm for JQ1-T). Images were captured after 30 min of incubation with the respective probe without washing. (d) The intensity analysis of JQ1-Th-TMR-Py in the Halo-NLS (nuclei) and non-transfected cells (cytosol): $N_{(Nuclei)}$ = 11 cells; $N_{(Cyto)}$ = 11 cells. (e) Schematic representation for the detection of EGFR targeting probes. (f) The structures of epidermal growth factor receptor−tyrosine kinase domain (EGFR−TKD)-targeting probes gefitinib-Th-TMR-Py (Gefi-T) and erlotinib-Th-TMR-Py (Erlo-T). (g) Live-cell imaging of endogenous EGFR with 5.0 μM Gefi-T on A431, HEK293T, or A431 after preincubation with 50 μM gefitinib (+Gefitinib(A431)). Cells were preincubated with 2.0 μM MitoTracker Deep Red for 10 min before the addition of the probe (λ_{ex} = 561 nm, λ_{em} = 580−610 nm for Gefi-T). (g) Fluorescence intensity analysis of the images of (h). The intensity analysis of Gefi-T in A431, HEK293T, and + Gefitinib(A431). $N_{(A431)}$ = 71 cells, $N_{(HEK293T)}$ = 70 cells, and $N_{(+Gefitinib(A431))}$ = 38 cells. (i) Live-cell imaging of A431 cells using Gefi-T upon gene knockdown using EGFR-targeting or non-EGFR-targeting siRNA. Cells were preincubated with 2.0 μM MitoTracker Deep Red for 10 min before the addition of the probe (λ_{ex} = 561 nm, λ_{em} = 580−610 nm for Gefi-T). Images were captured after 15 min of incubation of the respective probe without washing. PC: phase contrast.

to highlight the versatility of our fluorophores in live-cell protein imaging.

Fluorogenic Probe for BRD4. To develop a fluorogenic probe for intracellular protein detection, we selected BRD4, a key bromodomain and extraterminal (BET)[82] family protein involved in gene regulation through recognition of acetylated histones. BRD4 is a promising therapeutic target in cancer and inflammatory diseases.[83] Its significance is further underscored by the development of targeted protein degraders such as PROTACs and molecular glues that exploit BRD4 for selective degradation.[84] Its intracellular localization and biological relevance make it an ideal model target to demonstrate the capability of our non-covalent, fluorogenic probe for no-wash live-cell imaging (Figure 7a). To create a fluorogenic probe for BRD4, we conjugated the BRD4 inhibitor JQ1[85] to Th-TMR-Py-Acid via a short linker, forming the compound JQ1-Th-TMR-Py (JQ1-T) (Figure 7b and see supplementary discussion). To evaluate the ability to detect the BRD4 protein, we used a transient expression system to generate BRD4 in cells. NIH3T3 cells were transfected with the PYP^{wt}-BRD4[86] plasmid to introduce the protein to the cells. JQ1-T was incubated with PYP^{wt}-BRD4 expressing cells, which were pretreated with MTDR, and no-wash live-cell confocal imaging was conducted. Confocal fluorescence imaging data revealed that a bright fluorescence signal was detected in the nuclei of the cells (Figure 7c). However, non-transfected cells did not

https://doi.org/10.1021/jacs.5c12696
J. Am. Chem. Soc. 2025, 147, 47997−48012

exhibit any significant nuclear fluorescence signal (Figure 7c). Based on these findings, JQ1-T exhibited a 3.3-fold enhancement in fluorescence intensity in the nuclei of transfected cells compared to the cytosol of non-transfected cells (Figure 7d). This result indicates that JQ1-T is capable of detecting BRD4 in cells without washing. To confirm the nuclear expression of BRD4, we labeled the cells with C343-PYP, a green fluorogenic PYP probe, with JQ1-T (Figure S50a). The fluorescence signals from both probes showed perfect colocalization, further confirming that the observed fluorescence signal from JQ1-T originated from labeling BRD4 expressed in the cells (Figure S50b). For further verification, we preincubated the cells with 10 μM JQ1 and observed only negligible fluorescence. Fluorescence intensity analysis revealed a 4.4-fold decrease in fluorescence intensity upon the addition of JQ1 as a competitive unlabeled ligand (Figure S50c). This confirmed that the fluorescence signal originated specifically from binding of JQ1-T to BRD4 in the nuclei of the expressing cells, indicating its potential for detecting BRD4 expression that can be utilized for drug screening. Furthermore, we demonstrated that adding FCCP, a nonfluorescent additive, enhances target-specific detection of BRD4 expression (Figure S51).

EGFR-Targeting Fluorogenic Probes. We selected EGFR as the target for detection of membrane proteins with our fluorogenic probes because it is overexpressed in many cancer cells.[87] We developed novel fluorogenic probes by conjugating EGFR-targeting tyrosine kinase inhibitors (TKIs) gefitinib[88] and erlotinib[89] to Th-TMR-Py-Acid, resulting in gefitinib-Th-TMR-Py (Gefi-T) and erlotinib-Th-TMR-Py (Erlo-T), respectively (Figure 7e,f). The efficacy of the probes for detecting EGFR overexpression was evaluated in live A431 cells using a no-wash imaging protocol because of high expression of EGFR in the A431 cells.[89] Initially, Gefi-T and Erlo-T probes were mislocalized into mitochondria (Figure S52). However, the addition of MTDR enhanced the specificity and significantly improved the signal intensity for EGFR detection (Figures 7g and S53). Imaging data with Gefi-T and Erlo-T probes revealed strong fluorescence in A431 cells primarily at the cell membrane, while non-EGFR-overexpressing HEK293T cells showed a minimum fluorescence signal (Figures 7g and S53). Gefi-T exhibited a superior fluorogenic response compared to Erlo-T and was chosen for further experiments. Gefi-T detected 6.2-fold higher fluorescence intensity on the membrane of the A431 cells than the HEK293T cells (Figure 7h), and Western blot verified that the observed difference in the fluorescence intensities correlated with the difference in the EGFR expression levels in those cells (Figure S54). To confirm EGFR membrane expression, we performed colocalization imaging using Cetuximab-Alexa488 that binds to the extracellular domain of EGFR alongside intracellular tyrosine kinase domain (TKD)-binding Gefi-T (Figure S55). The overlap of green and red signals confirmed high EGFR expression on the membrane in A431 cells, whereas HEK293T cells showed minimum fluorescence in either channel under identical conditions. Additionally, immunostaining further verified high EGFR expression on the A431 cell membranes[90] (Figure S56), supporting our findings that the Gefi-T probe is capable of live-cell imaging using the no-wash imaging protocol.

To compare the EGFR detection ability of our fluorogenic probes with that of a spirolactam-based probe, we synthesized MaP555-Erlo by conjugating erlotinib with MaP555, a rhodamine fluorophore forming a spirolactam ring, and stained the cells under no-wash conditions. Fluorescence imaging revealed no fluorescence signal from intracellular compartments, with high background fluorescence signals from the extracellular media in both EGFR-expressing (A431) and non-expressing (HEK293T and MCF7) cells (Figures S57 and S58). These results indicate that MaP555-Erlo predominantly remains in the ring-opened form in the medium and does not produce detectable target signals due to its poor membrane permeability and high background fluorescence. This high background fluorescence impeded detection of the differences in the EGFR expression levels among the different cell types observed. A previous report also revealed that erlotinib-conjugated spirolactone probes were unable to detect EGFR in the A431 cell line.[70] These results indicate that the nature of the ligand or substituent attached to the fluorophore plays a crucial role in determining the fluorogenic behavior of spirocyclic and spirolactam-based probes.[91,92] Collectively, these findings highlight a key limitation of spirolactam-based probes that rely on ligand conjugation for their fluorogenic properties and emphasize the advantages of our fluorogenic TKI conjugates for the detection of EGFR in live cells.

To verify binding of Gefi-T to the TKD of EGFR, we preincubated the cells with 50 μM gefitinib before adding the probe. The result showed that the presence of gefitinib resulted in a 10-fold decrease in fluorescence signal in the A431 cells (Figure 7g,h),[93] indicating that binding of gefitinib competes with binding of Gefi-T to EGFR to reduce probe uptake and fluorescence signal intensity. Additionally, binding of Gefi-T to the TKD of EGFR was validated through an siRNA experiment conducted in A431 cells (Figure 7i), wherein a reduction in the EGFR signal was observed by both Gefi-T fluorescence measurements (Figure S59) and Western blotting (Figure S60) when EGFR-targeting siRNA was introduced to the cells. These findings confirm the specific binding of Gefi-T to EGFR and demonstrate that it can selectively detect the overexpression of EGFR intracellularly without washing, providing a valuable tool for monitoring EGFR expression levels.

CONCLUSIONS

In conclusion, we developed a novel class of fluorogenic fluorophores based on a xanthene core with finely tuned intramolecular rotation, achieved by introducing five-membered heterocycles such as furan or thiophene at the 9-position. This rotation-governed design enabled fluorescence activation upon interaction with biomolecular targets. The utility of this strategy was demonstrated by creating probes for self-labeling protein tags, such as HaloTag, SNAP-tag, and PYP-tag. Among them, HaloTag and PYP-tag probes showed excellent cell permeability and enabled efficient no-wash intracellular protein labeling in live cells. In particular, the sulfonated variant Th-TMR-S-Halo exhibited strong fluorogenic activation and high photostability, highlighting its potential for future nanoscopy research.

We demonstrated the practical utility of our HaloTag probes by monitoring real-time ER whorl formation during ER stress, highlighting their effectiveness in tracking protein dynamics in living cells. Expanding beyond covalent labeling, we developed the non-covalent probe JQ1-T for BRD4 detection. JQ1-T enabled fluorogenic imaging via an OFF−ON response upon BRD4 expression in live cells without washing, offering potential for drug screening and monitoring of protein overexpression.[18] Additionally, the EGFR-targeting probe Gefi-T showed strong membrane fluorescence in the EGFR-

https://doi.org/10.1021/jacs.5c12696
J. Am. Chem. Soc. 2025, 147, 47997−48012

overexpressing cells. The selectivity and sensitivity were validated by inhibitor treatments and siRNA knockdown, demonstrating the broad applicability of our design strategy for detecting EGFR across different cell lines. While the current BRD4 and EGFR probes benefit from the inclusion of MTDR as an additive, future structural optimization may improve their performance and eliminate the need for such additives. To deepen our understanding, we investigate the fluorogenic mechanism of these probes using advanced theoretical calculations, which may guide the development of next-generation fluorophores. Such new designs may not only enable precise modulation of fluorescence activation but also provide strong insight into the incorporation of other five-membered heterocycles to create improved and customizable probes. Overall, our approach expands the molecular toolkit for biomolecule detection in live cells and paves the way for future applications in biological and medical research.

■ ASSOCIATED CONTENT

Supporting Information

The Supporting Information is available free of charge at https://pubs.acs.org/doi/10.1021/jacs.5c12696.

Experimental details include synthetic procedure and characterization data of compounds, plasmid information, cell culture, confocal imaging, Western blotting, fluorescence spectra of fluorophores (2.5 μM) recorded in MeOH or glycerol, absorption spectra of fluorophores (10 μM) in MeOH and glycerol, absorption spectra of fluorophores (10 μM) in 20 mM HEPES buffer, absorption spectra of Th-CRhodol-Acid (10 μM) in 20 mM HEPES buffer, fluorescence spectra of fluorophores (2.5 μM) recorded in different solvents, fluorescence lifetime of fluorophores (2.5 μM) recorded in MeOH or glycerol, radiative (k_r) and non-radiative (k_{nr}) rate constants for Th-TMR-Acid and Ph-TMR-Acid, VT-NMR spectra of the aromatic region, fluorescence spectra of fluorophores (2.5 μM) recorded in various viscosities, absorption spectra of Th-TMR-Halo, Fu-CR-Halo, and Th-TMR-Py-Halo, absorption spectra of Th-TMR-Ju-Halo and Th-CR-Halo, fluorescence spectra and bar diagram of HaloTag probes (2.5 μM), Th-TMR-Halo, and Fu-CR-Halo in 20 mM HEPES buffer, SDS−PAGE analysis of labeling reactions between HaloTag probes, emission spectra of Th-TMR-Halo (2.5 μM) labeled with 5 μM HaloTag in HEPES buffer, excitation spectra and emission spectra of free Th-TMR-Halo, Th-TMR-Py-Halo, Th-CR-Halo, and Fu-CR-Halo, time-lapse fluorescence emission of HaloTag probes upon addition of two equivalence of HaloTag protein, live-cell imaging of Halo-NLS-expressing or non-transfected MCF7 cells using the no-wash protocol, chemical structures of Fu-CR-Halo and Th-CR-Halo, live-cell imaging of MCF7 cells expressing the gene for Halo-NLS using the no-wash imaging protocol, absorption spectra of Th-TMR-SNAP and Th-TMR-PYP, SDS−PAGE analysis of labeling reaction between SNAP-tag probes, absorption spectra of Th-TMR-Py-SNAP and Th-CR-SNAP, live-cell imaging of Th-TMR-SNAP, schematic representation of the photobleaching experiment, UV−vis spectra of Th-TMR-S-Acid (10.0 μM) in MeOH and glycerol, absorption and fluorescence emission spectra of Th-TMR-S-Halo, fluorescence spectra and bar diagram of Th-TMR-S-Halo, schematic representation of the protocol for the tag-labeling experiment, cell viabilities against Th-TMR-S-Halo and Th-TMR-S-SNAP, immunofluorescence images of A431 and HEK293T cells stained with an anti-EGFR primary antibody and anti-rabbit Alexa 488 as secondary antibody, UV−vis and fluorescence spectra of MaP555-Erlo, and mean fluorescence intensity of A431 using Gefi-T pretreated with 100 nM non-targeting or EGFR targeting siRNA (PDF)

■ AUTHOR INFORMATION

Corresponding Authors

Yuichiro Hori − *Department of Chemistry, Graduate School of Science, Kyushu University, Fukuoka 819-0395, Japan*; Email: hori@chem.kyushu-univ.jp

Kazuya Kikuchi − *Immunology Frontier Research Center (WPI-IFReC), The University of Osaka, Suita, Osaka 565-0871, Japan; Department of Applied Chemistry, Graduate School of Engineering, The University of Osaka, Suita, Osaka 565-0871, Japan;* orcid.org/0000-0001-7103-1275; Email: kkikuchi@mls.eng.osaka-u.ac.jp

Authors

Shahi Imam Reja − *Immunology Frontier Research Center (WPI-IFReC), The University of Osaka, Suita, Osaka 565-0871, Japan;* orcid.org/0000-0003-2287-3817

Youhei Takeda − *Department of Applied Chemistry, Graduate School of Engineering, The University of Osaka, Suita, Osaka 565-0871, Japan;* orcid.org/0000-0001-9103-4238

Miyako Nishiura − *Department of Applied Chemistry, Graduate School of Engineering, The University of Osaka, Suita, Osaka 565-0871, Japan*

Masafumi Minoshima − *Department of Applied Chemistry, Graduate School of Engineering, The University of Osaka, Suita, Osaka 565-0871, Japan; JST, Suita, Osaka 565-0871, Japan;* orcid.org/0000-0002-9352-3454

Complete contact information is available at: https://pubs.acs.org/10.1021/jacs.5c12696

Author Contributions

The manuscript was written through contributions of all authors.

Notes

The authors declare no competing financial interest.

■ ACKNOWLEDGMENTS

This work was supported by the IFReC advanced postdoc program (S.I.R. and K.K.). This work was also supported by a Grant-in-Aid for Transformative Research Area (A) "Latent Chemical Space" [23H04880 and 23H04881 (K.K.)] from the Ministry of Education, Culture, Sports, Science and Technology, Japan. This research was also supported by JSPS KAKENHI (grant numbers: JP21H04706 and JP23KK0106 to K.K.; JP20H02879, JP21K19048, and JP21H05075 to Y.H.; JP20K05747, JP21H00401, and JP22H05425 to M.M.); JST PRESTO (JPMJPR22EC to M.M.); the JSPS CORE-to-CORE Program "Asian Chemical Biology Initiative"; and the Collaborative Research Program of Institute for Chemical Research, Kyoto University (2025-88 to K.K.). The parts of

the schematic illustrations in the figures were created with BioRender.com. We thank the analytical instrument facility, Graduate School of Engineering, the University of Osaka, for HRMS analysis; Nikon Imaging Center (NIC), the University of Osaka, for AX R with NSPARC (Nikon Spatial Array Confocal) Inverted-type Confocal-based Super-Resolution Microscope and Super-Resolution Structured Illumination Microscope (N-SIM).

REFERENCES

(1) Lukinavičius, G.; Reymond, L.; D'Este, E.; Masharina, A.; Göttfert, F.; Ta, H.; Güther, A.; Fournier, M.; Rizzo, S.; Waldmann, H.; Blaukopf, C.; Sommer, C.; Gerlich, D. W.; Arndt, H.-D.; Hell, S. W.; Johnsson, K. Fluorogenic probes for live-cell imaging of the cytoskeleton. *Nat. Methods* **2014**, *11* (7), 731−733.

(2) Reese, A. E.; de Moliner, F.; Mendive-Tapia, L.; Benson, S.; Kuru, E.; Bridge, T.; Richards, J.; Rittichier, J.; Kitamura, T.; Sachdeva, A.; McSorley, H. J.; Vendrell, M. Inserting "OFF-to-ON" BODIPY Tags into Cytokines: A Fluorogenic Interleukin IL-33 for Real-Time Imaging of Immune Cells. *ACS Cent. Sci.* **2024**, *10* (1), 143−154.

(3) Chang, H.; Clemens, S.; Gao, P.; Li, Q.; Zhao, H.; Wang, L.; Zhang, J.; Zhou, P.; Johnsson, K.; Wang, L. Fluorogenic Rhodamine-Based Chemigenetic Biosensor for Monitoring Cellular NADPH Dynamics. *J. Am. Chem. Soc.* **2024**, *146* (30), 20569−20576.

(4) Werther, P.; Yserentant, K.; Braun, F.; Grußmayer, K.; Navikas, V.; Yu, M.; Zhang, Z.; Ziegler, M. J.; Mayer, C.; Gralak, A. J.; Busch, M.; Chi, W.; Rominger, F.; Radenovic, A.; Liu, X.; Lemke, E. A.; Buckup, T.; Herten, D.-P.; Wombacher, R. Bio-Orthogonal Red and Far-Red Fluorogenic Probes for Wash-Free Live-Cell and Super-Resolution Microscopy. *ACS Cent. Sci.* **2021**, *7* (9), 1561−1571.

(5) Los, G. V.; Encell, L. P.; McDougall, M. G.; Hartzell, D. D.; Karassina, N.; Zimprich, C.; Wood, M. G.; Learish, R.; Ohana, R. F.; Urh, M.; Simpson, D.; Mendez, J.; Zimmerman, K.; Otto, P.; Vidugiris, G.; Zhu, J.; Darzins, A.; Klaubert, D. H.; Bulleit, R. F.; Wood, K. V. HaloTag: A Novel Protein Labeling Technology for Cell Imaging and Protein Analysis. *ACS Chem. Biol.* **2008**, *3* (6), 373−382.

(6) Keppler, A.; Gendreizig, S.; Gronemeyer, T.; Pick, H.; Vogel, H.; Johnsson, K. A General Method for the Covalent Labeling of Fusion Proteins with Small Molecules in Vivo. *Nat. Biotechnol.* **2003**, *21* (1), 86−89.

(7) Hirayama, S.; Hori, Y.; Benedek, Z.; Suzuki, T.; Kikuchi, K. Fluorogenic Probes Reveal a Role of GLUT4 N-Glycosylation in Intracellular Trafficking. *Nat. Chem. Biol.* **2016**, *12* (10), 853−859.

(8) Lincoln, R.; Bossi, M. L.; Remmel, M.; D'Este, E.; Butkevich, A. N.; Hell, S. W. A General Design of Caging-Group-Free Photoactivatable Fluorophores for Live-Cell Nanoscopy. *Nat. Chem.* **2022**, *14* (9), 1013−1020.

(9) Minoshima, M.; Reja, S. I.; Hashimoto, R.; Iijima, K.; Kikuchi, K. Hybrid Small-Molecule/Protein Fluorescent Probes. *Chem. Rev.* **2024**, *124* (10), 6198−6270.

(10) Lukinavičius, G.; Umezawa, K.; Olivier, N.; Honigmann, A.; Yang, G.; Plass, T.; Mueller, V.; Reymond, L.; Corrêa, I. R., Jr; Luo, Z.-G.; Schultz, C.; Lemke, E. A.; Heppenstall, P.; Eggeling, C.; Manley, S.; Johnsson, K. A Near-Infrared Fluorophore for Live-Cell Super-Resolution Microscopy of Cellular Proteins. *Nat. Chem.* **2013**, *5* (2), 132−139.

(11) Martin, A.; Rivera-Fuentes, P. A General Strategy to Develop Fluorogenic Polymethine Dyes for Bioimaging. *Nat. Chem.* **2024**, *16* (1), 28−35.

(12) Wang, L.; Tran, M.; D'Este, E.; Roberti, J.; Koch, B.; Xue, L.; Johnsson, K. A General Strategy to Develop Cell Permeable and Fluorogenic Probes for Multicolour Nanoscopy. *Nat. Chem.* **2020**, *12* (2), 165−172.

(13) Bertolini, M.; Mendive-Tapia, L.; Ghashghaei, O.; Reese, A.; Lochenie, C.; Schoepf, A. M.; Sintes, M.; Tokarczyk, K.; Nare, Z.; Scott, A. D.; Knight, S. R.; Aithal, A. R.; Sachdeva, A.; Lavilla, R.; Vendrell, M. Nonperturbative Fluorogenic Labeling of Immunophilins Enables the Wash-Free Detection of Immunosuppressants. *ACS Cent. Sci.* **2024**, *10* (5), 969−977.

(14) Zheng, Q.; Ayala, A. X.; Chung, I.; Weigel, A. V.; Ranjan, A.; Falco, N.; Grimm, J. B.; Tkachuk, A. N.; Wu, C.; Lippincott-Schwartz, J.; Singer, R. H.; Lavis, L. D. Rational Design of Fluorogenic and Spontaneously Blinking Labels for Super-Resolution Imaging. *ACS Cent. Sci.* **2019**, *5* (9), 1602−1613.

(15) Mao, W.; Tang, J.; Dai, L.; He, X.; Li, J.; Cai, L.; Liao, P.; Jiang, R.; Zhou, J.; Wu, H. A General Strategy to Design Highly Fluorogenic Far-Red and near-Infrared Tetrazine Bioorthogonal Probes. *Angew. Chem., Int. Ed. Engl.* **2021**, *60* (5), 2393−2397.

(16) Yu, A.; He, X.; Shen, T.; Yu, X.; Mao, W.; Chi, W.; Liu, X.; Wu, H. Design Strategies for Tetrazine Fluorogenic Probes for Bioorthogonal Imaging. *Chem. Soc. Rev.* **2025**, *54* (6), 2984−3016.

(17) Reja, S. I.; Minoshima, M.; Hori, Y.; Kikuchi, K. Recent Advancements of Fluorescent Biosensors Using Semisynthetic Probes. *Biosens. Bioelectron.* **2024**, *247* (115862), 115862.

(18) Li, T.; Zong, Q.; Dong, H.; Ullah, I.; Pan, Z.; Yuan, Y. Non-Invasive in Vivo Monitoring of PROTAC-Mediated Protein Degradation Using an Environment-Sensitive Reporter. *Nat. Commun.* **2025**, *16* (1), 1892.

(19) Sato, R.; Kozuka, J.; Ueda, M.; Mishima, R.; Kumagai, Y.; Yoshimura, A.; Minoshima, M.; Mizukami, S.; Kikuchi, K. Intracellular Protein-Labeling Probes for Multicolor Single-Molecule Imaging of Immune Receptor-Adaptor Molecular Dynamics. *J. Am. Chem. Soc.* **2017**, *139* (48), 17397−17404.

(20) Likhotkin, I.; Lincoln, R.; Bossi, M. L.; Butkevich, A. N.; Hell, S. W. Photoactivatable Large Stokes Shift Fluorophores for Multicolor Nanoscopy. *J. Am. Chem. Soc.* **2023**, *145* (3), 1530−1534.

(21) Niu, H.; Liu, J.; O'Connor, H. M.; Gunnlaugsson, T.; James, T. D.; Zhang, H. Photoinduced Electron Transfer (PeT) Based Fluorescent Probes for Cellular Imaging and Disease Therapy. *Chem. Soc. Rev.* **2023**, *52* (7), 2322−2357.

(22) Faucher, F. F.; Liu, K. J.; Cosco, E. D.; Widen, J. C.; Sorger, J.; Guerra, M.; Bogyo, M. Protease Activated Probes for Real-Time Ratiometric Imaging of Solid Tumors. *ACS Cent. Sci.* **2023**, *9* (5), 1059−1069.

(23) Suzuki, Y.; Yokoyama, K. Design and Synthesis of Intramolecular Charge Transfer-Based Fluorescent Reagents for the Highly-Sensitive Detection of Proteins. *J. Am. Chem. Soc.* **2005**, *127* (50), 17799−17802.

(24) Hanaoka, K.; Ikeno, T.; Iwaki, S.; Deguchi, S.; Takayama, K.; Mizuguchi, H.; Tao, F.; Kojima, N.; Ohno, H.; Sasaki, E.; Komatsu, T.; Ueno, T.; Maeda, K.; Kusuhara, H.; Urano, Y. A General Fluorescence off/on Strategy for Fluorogenic Probes: Steric Repulsion-Induced Twisted Intramolecular Charge Transfer (Sr-TICT). *Sci. Adv.* **2024**, *10* (7), No. eadi8847.

(25) Huang, R.; Qiao, Q.; Seah, D.; Shen, T.; Wu, X.; de Moliner, F.; Wang, C.; Ding, N.; Chi, W.; Sun, H.; Vendrell, M.; Xu, Z.; Fang, Y.; Liu, X. Precision Molecular Engineering of Compact Near-Infrared Fluorophores. *J. Am. Chem. Soc.* **2025**, *147* (6), 5258−5268.

(26) Si, D.; Li, Q.; Bao, Y.; Zhang, J.; Wang, L. Fluorogenic and Cell-Permeable Rhodamine Dyes for High-Contrast Live-Cell Protein Labeling in Bioimaging and Biosensing. *Angew. Chem., Int. Ed. Engl.* **2023**, *62* (45), No. e202307641.

(27) Ceresole, M. Verfahren zur Darstellung von Farbstoffenaus der Gruppe des Meta-amidophenol-Phtaleins. 44002, 1887.

(28) Schnermann, M. J.; Lavis, L. D. Rejuvenating Old Fluorophores with New Chemistry. *Curr. Opin. Chem. Biol.* **2023**, *75* (102335), 102335.

(29) Lavis, L. D.; Raines, R. T. Bright Ideas for Chemical Biology. *ACS Chem. Biol.* **2008**, *3* (3), 142−155.

(30) Koide, Y.; Urano, Y.; Hanaoka, K.; Terai, T.; Nagano, T. Evolution of Group 14 Rhodamines as Platforms for Near-Infrared Fluorescence Probes Utilizing Photoinduced Electron Transfer. *ACS Chem. Biol.* **2011**, *6* (6), 600−608.

(31) Lardon, N.; Wang, L.; Tschanz, A.; Hoess, P.; Tran, M.; D'Este, E.; Ries, J.; Johnsson, K. Systematic Tuning of Rhodamine

https://doi.org/10.1021/jacs.5c12696
J. Am. Chem. Soc. 2025, 147, 47997−48012

Spirocyclization for Super-Resolution Microscopy. *J. Am. Chem. Soc.* **2021**, *143* (36), 14592−14600.
(32) Wang, L.; Hiblot, J.; Popp, C.; Xue, L.; Johnsson, K. Environmentally Sensitive Color-Shifting Fluorophores for Bioimaging. *Angew. Chem., Int. Ed. Engl.* **2020**, *59* (49), 21880−21884.
(33) Fang, X.; Qiao, Q.; Li, Z.; Li, H.-K.; Huang, Y.; Hou, D.; Chen, J.; Xu, N.; An, K.; Jiang, W.; Tao, Y.; Bao, P.; Zhang, Y.; Wu, Z.; Liu, X.; Xu, Z. Ether Rhodamines with Enhanced Hydrophilicity, Fluorogenicity, and Brightness for Super-Resolution Imaging. *J. Am. Chem. Soc.* **2025**, *147* (25), 22253−22267.
(34) Grimm, J. B.; Tkachuk, A. N.; Patel, R.; Hennigan, S. T.; Gutu, A.; Dong, P.; Gandin, V.; Osowski, A. M.; Holland, K. L.; Liu, Z. J.; Brown, T. A.; Lavis, L. D. Optimized Red-Absorbing Dyes for Imaging and Sensing. *J. Am. Chem. Soc.* **2023**, *145* (42), 23000−23013.
(35) Grimm, J. B.; Tkachuk, A. N.; Xie, L.; Choi, H.; Mohar, B.; Falco, N.; Schaefer, K.; Patel, R.; Zheng, Q.; Liu, Z.; Lippincott-Schwartz, J.; Brown, T. A.; Lavis, L. D. A General Method to Optimize and Functionalize Red-Shifted Rhodamine Dyes. *Nat. Methods* **2020**, *17* (8), 815−821.
(36) Zhang, J.; Zhang, K.; Wang, K.; Wang, B.; Zhu, S.; Qian, H.; Ma, Y.; Zhang, M.; Liu, T.; Chen, P.; Shen, Y.; Fu, Y.; Fang, S.; Zhang, X.; Zou, P.; Deng, W.; Mu, Y.; Chen, Z. A Palette of Bridged Bicycle-Strengthened Fluorophores. *Nat. Methods* **2025**, *22* (6), 1276−1287.
(37) Ramette, R. W.; Sandell, E. B. Rhodamine B Equilibria. *J. Am. Chem. Soc.* **1956**, *78* (19), 4872−4878.
(38) Lee, M. K.; Rai, P.; Williams, J.; Twieg, R. J.; Moerner, W. E. Small-Molecule Labeling of Live Cell Surfaces for Three-Dimensional Super-Resolution Microscopy. *J. Am. Chem. Soc.* **2014**, *136* (40), 14003−14006.
(39) Chen, X.; Pradhan, T.; Wang, F.; Kim, J. S.; Yoon, J. Fluorescent Chemosensors Based on Spiroring-Opening of Xanthenes and Related Derivatives. *Chem. Rev.* **2012**, *112* (3), 1910−1956.
(40) Grimm, J. B.; Muthusamy, A. K.; Liang, Y.; Brown, T. A.; Lemon, W. C.; Patel, R.; Lu, R.; Macklin, J. J.; Keller, P. J.; Ji, N.; Lavis, L. D. A General Method to Fine-Tune Fluorophores for Live-Cell and in Vivo Imaging. *Nat. Methods* **2017**, *14* (10), 987−994.
(41) Lukinavičius, G.; Mitronova, G. Y.; Schnorrenberg, S.; Butkevich, A. N.; Barthel, H.; Belov, V. N.; Hell, S. W. Fluorescent Dyes and Probes for Super-Resolution Microscopy of Microtubules and Tracheoles in Living Cells and Tissues. *Chem. Sci.* **2018**, *9* (13), 3324−3334.
(42) Kikuchi, K.; Adair, L. D.; Lin, J.; New, E. J.; Kaur, A. Photochemical Mechanisms of Fluorophores Employed in Single-Molecule Localization Microscopy. *Angew. Chem., Int. Ed. Engl.* **2023**, *62* (1), No. e202204745.
(43) Minoshima, M.; Kikuta, J.; Omori, Y.; Seno, S.; Suehara, R.; Maeda, H.; Matsuda, H.; Ishii, M.; Kikuchi, K. In Vivo Multicolor Imaging with Fluorescent Probes Revealed the Dynamics and Function of Osteoclast Proton Pumps. *ACS Cent. Sci.* **2019**, *5* (6), 1059−1066.
(44) Hanaoka, K.; Iwaki, S.; Yagi, K.; Myochin, T.; Ikeno, T.; Ohno, H.; Sasaki, E.; Komatsu, T.; Ueno, T.; Uchigashima, M.; Mikuni, T.; Tainaka, K.; Tahara, S.; Takeuchi, S.; Tahara, T.; Uchiyama, M.; Nagano, T.; Urano, Y. General Design Strategy to Precisely Control the Emission of Fluorophores via a Twisted Intramolecular Charge Transfer (TICT) Process. *J. Am. Chem. Soc.* **2022**, *144* (43), 19778−19790.
(45) Xu, F.; Du, W.; Zou, Q.; Wang, Y.; Zhang, X.; Xing, X.; Li, Y.; Zhang, D.; Wang, H.; Zhang, W.; Hu, X.; Liu, X.; Liu, X.; Zhang, S.; Yu, J.; Fang, J.; Li, F.; Zhou, Y.; Yue, T.; Mi, N.; Deng, H.; Zou, P.; Chen, X.; Yang, X.; Yu, L. COPII Mitigates ER Stress by Promoting Formation of ER Whorls. *Cell Res.* **2021**, *31* (2), 141−156.
(46) Sigismund, S.; Avanzato, D.; Lanzetti, L. Emerging Functions of the EGFR in Cancer. *Mol. Oncol.* **2018**, *12* (1), 3−20.
(47) Donati, B.; Lorenzini, E.; Ciarrocchi, A. BRD4 and Cancer: Going beyond Transcriptional Regulation. *Mol. Cancer* **2018**, *17* (1), 164.
(48) Lindqvist, L.; Lundeen, G. W. Radiationless Transitions in Xanthene Dyes. *J. Chem. Phys.* **1966**, *44* (4), 1711−1712.
(49) Fink, D. W.; Willis, C. R. Structure and Internal Mixing in Xanthene Dyes. *J. Chem. Phys.* **1970**, *53* (12), 4720−4722.
(50) Urano, Y.; Kamiya, M.; Kanda, K.; Ueno, T.; Hirose, K.; Nagano, T. Evolution of Fluorescein as a Platform for Finely Tunable Fluorescence Probes. *J. Am. Chem. Soc.* **2005**, *127* (13), 4888−4894.
(51) Arambula, C.; Rodrigues, J.; Koh, J. J.; Woydziak, Z. Synthesis of Rhodamines and Rosamines Using 3,6-Difluoroxanthone as a Common Intermediate. *J. Org. Chem.* **2021**, *86* (24), 17856−17865.
(52) Vyšniauskas, A.; López-Duarte, I.; Duchemin, N.; Vu, T.-T.; Wu, Y.; Budynina, E. M.; Volkova, Y. A.; Peña Cabrera, E.; Ramírez-Ornelas, D. E.; Kuimova, M. K. Exploring Viscosity, Polarity and Temperature Sensitivity of BODIPY-Based Molecular Rotors. *Phys. Chem. Chem. Phys.* **2017**, *19* (37), 25252−25259.
(53) Sinkeldam, R. W.; Wheat, A. J.; Boyaci, H.; Tor, Y. Emissive Nucleosides as Molecular Rotors. *ChemPhysChem* **2011**, *12* (3), 567−570.
(54) Cservenyi, T. Z.; Van Riesen, A. J.; Berger, F. D.; Desoky, A.; Manderville, R. A. A Simple Molecular Rotor for Defining Nucleoside Environment within a DNA Aptamer-Protein Complex. *ACS Chem. Biol.* **2016**, *11* (9), 2576−2582.
(55) Grimm, J. B.; English, B. P.; Chen, J.; Slaughter, J. P.; Zhang, Z.; Revyakin, A.; Patel, R.; Macklin, J. J.; Normanno, D.; Singer, R. H.; Lionnet, T.; Lavis, L. D. A General Method to Improve Fluorophores for Live-Cell and Single-Molecule Microscopy. *Nat. Methods* **2015**, *12* (3), 244−250.
(56) Haidekker, M. A.; Theodorakis, E. A. Molecular Rotors-Fluorescent Biosensors for Viscosity and Flow. *Org. Biomol. Chem.* **2007**, *5* (11), 1669−1678.
(57) Raut, S.; Kimball, J.; Fudala, R.; Doan, H.; Maliwal, B.; Sabnis, N.; Lacko, A.; Gryczynski, I.; Dzyuba, S. V.; Gryczynski, Z. A Homodimeric BODIPY Rotor as a Fluorescent Viscosity Sensor for Membrane-Mimicking and Cellular Environments. *Phys. Chem. Chem. Phys.* **2014**, *16* (48), 27037−27042.
(58) Umezawa, K.; Yoshida, M.; Kamiya, M.; Yamasoba, T.; Urano, Y. Rational Design of Reversible Fluorescent Probes for Live-Cell Imaging and Quantification of Fast Glutathione Dynamics. *Nat. Chem.* **2017**, *9* (3), 279−286.
(59) Haidekker, M. A.; Theodorakis, E. A. Environment-Sensitive Behavior of Fluorescent Molecular Rotors. *J. Biol. Eng.* **2010**, *4* (1), 11.
(60) Jin, Y.-J.; Park, H.; Ohk, Y.-J.; Kwak, G. Hydrodynamic Fluorescence Emission Behavior of Molecular Rotor-Based Vinyl Polymers Used as Viscosity Sensors. *Polymer* **2017**, *132*, 79−87.
(61) Liu, X.; Chi, W.; Qiao, Q.; Kokate, S. V.; Cabrera, E. P.; Xu, Z.; Liu, X.; Chang, Y.-T. Molecular Mechanism of Viscosity Sensitivity in BODIPY Rotors and Application to Motion-Based Fluorescent Sensors. *ACS Sens.* **2020**, *5* (3), 731−739.
(62) Reja, S. I.; Hori, Y.; Kamikawa, T.; Yamasaki, K.; Nishiura, M.; Bull, S. D.; Kikuchi, K. An "OFF-ON-OFF" Fluorescence Protein-Labeling Probe for Real-Time Visualization of the Degradation of Short-Lived Proteins in Cellular Systems. *Chem. Sci.* **2022**, *13* (5), 1419−1427.
(63) Wang, B.; Zhao, Z.; Xiong, M.; Yan, R.; Xu, K. The Endoplasmic Reticulum Adopts Two Distinct Tubule Forms. *Proc. Natl. Acad. Sci. U.S.A.* **2022**, *119* (18), No. e2117559119.
(64) Torii, K.; Benson, S.; Hori, Y.; Vendrell, M.; Kikuchi, K. No-Wash Fluorogenic Labeling of Proteins for Reversible Photoswitching in Live Cells. *Chem. Sci.* **2024**, *15* (4), 1393−1401.
(65) Hori, Y.; Otomura, N.; Nishida, A.; Nishiura, M.; Umeno, M.; Suetake, I.; Kikuchi, K. Synthetic-Molecule/Protein Hybrid Probe with Fluorogenic Switch for Live-Cell Imaging of DNA Methylation. *J. Am. Chem. Soc.* **2018**, *140* (5), 1686−1690.
(66) Perry, S. W.; Norman, J. P.; Barbieri, J.; Brown, E. B.; Gelbard, H. A. Mitochondrial Membrane Potential Probes and the Proton Gradient: A Practical Usage Guide. *Biotechniques* **2011**, *50* (2), 98−115.

https://doi.org/10.1021/jacs.5c12696
J. Am. Chem. Soc. 2025, 147, 47997−48012

(67) Nishiura, M.; Hori, Y.; Umeno, M.; Kikuchi, K. Visualization of Multiple Localizations of GLUT4 by Fluorescent Probes of PYP-Tag with Designed Unnatural Warhead. *Chem. Sci.* **2023**, *14* (22), 5925−5935.
(68) Li, C.; Plamont, M.-A.; Sladitschek, H. L.; Rodrigues, V.; Aujard, I.; Neveu, P.; Le Saux, T.; Jullien, L.; Gautier, A. Dynamic Multicolor Protein Labeling in Living Cells. *Chem. Sci.* **2017**, *8* (8), 5598−5605.
(69) Berlier, J. E.; Rothe, A.; Buller, G.; Bradford, J.; Gray, D. R.; Filanoski, B. J.; Telford, W. G.; Yue, S.; Liu, J.; Cheung, C.-Y.; Chang, W.; Hirsch, J. D.; Beechem Rosaria P Haugland, J. M.; Haugland, R. P.; Haugland, R. P. Quantitative Comparison of Long-Wavelength Alexa Fluor Dyes to Cy Dyes: Fluorescence of the Dyes and Their Bioconjugates. *J. Histochem. Cytochem.* **2003**, *51* (12), 1699−1712.
(70) Wang, L. G.; Montaño, A. R.; Combs, J. R.; McMahon, N. P.; Solanki, A.; Gomes, M. M.; Tao, K.; Bisson, W. H.; Szafran, D. A.; Samkoe, K. S.; Tichauer, K. M.; Gibbs, S. L. OregonFluor Enables Quantitative Intracellular Paired Agent Imaging to Assess Drug Target Availability in Live Cells and Tissues. *Nat. Chem.* **2023**, *15* (5), 729−739.
(71) Kühn, S.; Nasufovic, V.; Wilhelm, J.; Kompa, J.; de Lange, E. M. F.; Lin, Y.-H.; Egoldt, C.; Fischer, J.; Lennoi, A.; Tarnawski, M.; Reinstein, J.; Vlijm, R.; Hiblot, J.; Johnsson, K. SNAP-Tag2 for Faster and Brighter Protein Labeling. *Nat. Chem. Biol.* **2025**, *21* (11), 1754−1761.
(72) Uno, S.-N.; Kamiya, M.; Yoshihara, T.; Sugawara, K.; Okabe, K.; Tarhan, M. C.; Fujita, H.; Funatsu, T.; Okada, Y.; Tobita, S.; Urano, Y. A Spontaneously Blinking Fluorophore Based on Intramolecular Spirocyclization for Live-Cell Super-Resolution Imaging. *Nat. Chem.* **2014**, *6* (8), 681−689.
(73) Mo, J.; Chen, J.; Shi, Y.; Sun, J.; Wu, Y.; Liu, T.; Zhang, J.; Zheng, Y.; Li, Y.; Chen, Z. Third-Generation Covalent TMP-Tag for Fast Labeling and Multiplexed Imaging of Cellular Proteins. *Angew. Chem., Int. Ed. Engl.* **2022**, *61* (36), No. e202207905.
(74) Butkevich, A. N.; Mitronova, G. Y.; Sidenstein, S. C.; Klocke, J. L.; Kamin, D.; Meineke, D. N. H.; D'Este, E.; Kraemer, P.-T.; Danzl, J. G.; Belov, V. N.; Hell, S. W. *Angew. Chem., Int. Ed.* **2016**, *55*, 3290−3294.
(75) Delattre, S. Igniting New Confocal Imaging Potential - Nikon AX R Series with NSPARC. *Microsc. Today* **2023**, *31* (6), 23−27.
(76) Gustafsson, M. G. Surpassing the Lateral Resolution Limit by a Factor of Two Using Structured Illumination Microscopy. *J. Microsc.* **2000**, *198*, 82−87.
(77) Brodsky, J. L. Cleaning up: ER-Associated Degradation to the Rescue. *Cell* **2012**, *151* (6), 1163−1167.
(78) Wiseman, R. L.; Mesgarzadeh, J. S.; Hendershot, L. M. Reshaping Endoplasmic Reticulum Quality Control through the Unfolded Protein Response. *Mol. Cell* **2022**, *82* (8), 1477−1491.
(79) Chen, G.; Wei, T.; Ju, F.; Li, H. Protein Quality Control and Aggregation in the Endoplasmic Reticulum: From Basic to Bedside. *Front. Cell Dev. Biol.* **2023**, *11*, 1156152.
(80) Xu, F.; Du, W.; Zou, Q.; Wang, Y.; Zhang, X.; Xing, X.; Li, Y.; Zhang, D.; Wang, H.; Zhang, W.; Hu, X.; Liu, X.; Liu, X.; Zhang, S.; Yu, J.; Fang, J.; Li, F.; Zhou, Y.; Yue, T.; Mi, N.; Deng, H.; Zou, P.; Chen, X.; Yang, X.; Yu, L. COPII Mitigates ER Stress by Promoting Formation of ER Whorls. *Cell Res.* **2021**, *31* (2), 141−156.
(81) Guo, Y.; Shen, D.; Zhou, Y.; Yang, Y.; Liang, J.; Zhou, Y.; Li, N.; Liu, Y.; Yang, G.; Li, W. Deep Learning-Based Morphological Classification of Endoplasmic Reticulum under Stress. *Front. Cell Dev. Biol.* **2022**, *9*, 767866.
(82) Wang, Z.-Q.; Zhang, Z.-C.; Wu, Y.-Y.; Pi, Y.-N.; Lou, S.-H.; Liu, T.-B.; Lou, G.; Yang, C. Bromodomain and Extraterminal (BET) Proteins: Biological Functions, Diseases, and Targeted Therapy. *Signal Transduct. Targeted Ther.* **2023**, *8* (1), 420.
(83) Devaiah, B. N.; Case-Borden, C.; Gegonne, A.; Hsu, C. H.; Chen, Q.; Meerzaman, D.; Dey, A.; Ozato, K.; Singer, D. S. BRD4 Is a Histone Acetyltransferase That Evicts Nucleosomes from Chromatin. *Nat. Struct. Mol. Biol.* **2016**, *23* (6), 540−548.
(84) Bhela, I. P.; Ranza, A.; Balestrero, F. C.; Serafini, M.; Aprile, S.; Di Martino, R. M. C.; Condorelli, F.; Pirali, T. A Versatile and Sustainable Multicomponent Platform for the Synthesis of Protein Degraders: Proof-of-Concept Application to BRD4-Degrading PROTACs. *J. Med. Chem.* **2022**, *65* (22), 15282−15299.
(85) Filippakopoulos, P.; Qi, J.; Picaud, S.; Shen, Y.; Smith, W. B.; Fedorov, O.; Morse, E. M.; Keates, T.; Hickman, T. T.; Felletar, I.; Philpott, M.; Munro, S.; McKeown, M. R.; Wang, Y.; Christie, A. L.; West, N.; Cameron, M. J.; Schwartz, B.; Heightman, T. D.; La Thangue, N.; French, C. A.; Wiest, O.; Kung, A. L.; Knapp, S.; Bradner, J. E. Selective Inhibition of BET Bromodomains. *Nature* **2010**, *468* (7327), 1067−1073.
(86) Hori, Y.; Hirayama, S.; Sato, M.; Kikuchi, K. Redesign of a Fluorogenic Labeling System to Improve Surface Charge, Brightness, and Binding Kinetics for Imaging the Functional Localization of Bromodomains. *Angew. Chem., Int. Ed. Engl.* **2015**, *54* (48), 14368−14371.
(87) Selvaggi, G.; Novello, S.; Torri, V.; Leonardo, E.; De Giuli, P.; Borasio, P.; Mossetti, C.; Ardissone, F.; Lausi, P.; Scagliotti, G. V. Epidermal Growth Factor Receptor Overexpression Correlates with a Poor Prognosis in Completely Resected Non-Small-Cell Lung Cancer. *Ann. Oncol.* **2004**, *15* (1), 28−32.
(88) Pao, W.; Miller, V.; Zakowski, M.; Doherty, J.; Politi, K.; Sarkaria, I.; Singh, B.; Heelan, R.; Rusch, V.; Fulton, L.; Mardis, E.; Kupfer, D.; Wilson, R.; Kris, M.; Varmus, H. EGF Receptor Gene Mutations Are Common in Lung Cancers from "Never Smokers" and Are Associated with Sensitivity of Tumors to Gefitinib and Erlotinib. *Proc. Natl. Acad. Sci. U.S.A.* **2004**, *101* (36), 13306−13311.
(89) Merlino, G. T.; Xu, Y. H.; Ishii, S.; Clark, A. J.; Semba, K.; Toyoshima, K.; Yamamoto, T.; Pastan, I. Amplification and Enhanced Expression of the Epidermal Growth Factor Receptor Gene in A431 Human Carcinoma Cells. *Science* **1984**, *224* (4647), 417−419.
(90) Pinilla-Macua, I.; Grassart, A.; Duvvuri, U.; Watkins, S. C.; Sorkin, A. EGF Receptor Signaling, Phosphorylation, Ubiquitylation and Endocytosis in Tumors in Vivo. *Elife* **2017**, *6*, No. e31993.
(91) Kompa, J.; Bruins, J.; Glogger, M.; Wilhelm, J.; Frei, M. S.; Tarnawski, M.; D'Este, E.; Heilemann, M.; Hiblot, J.; Johnsson, K. Exchangeable HaloTag Ligands for Super-Resolution Fluorescence Microscopy. *J. Am. Chem. Soc.* **2023**, *145* (5), 3075−3083.
(92) Birke, R.; Ast, J.; Roosen, D. A.; Lee, J.; Roßmann, K.; Huhn, C.; Mathes, B.; Lisurek, M.; Bushiri, D.; Sun, H.; Jones, B.; Lehmann, M.; Levitz, J.; Haucke, V.; Hodson, D. J.; Broichhagen, J. Sulfonated Red and Far-Red Rhodamines to Visualize SNAP- and Halo-Tagged Cell Surface Proteins. *Org. Biomol. Chem.* **2022**, *20* (30), 5967−5980.
(93) Deng, H.; Lei, Q.; Wang, C.; Wang, Z.; Chen, H.; Wang, G.; Yang, N.; Huang, D.; Yu, Q.; Yao, M.; Xiao, X.; Zhu, G.; Cheng, C.; Li, Y.; Li, F.; Tian, P.; Li, W. A Fluorogenic Probe for Predicting Treatment Response in Non-Small Cell Lung Cancer with EGFR-Activating Mutations. *Nat. Commun.* **2022**, *13* (1), 6944.

https://doi.org/10.1021/jacs.5c12696
J. Am. Chem. Soc. 2025, 147, 47997−48012